AD-A122 552 CORONA PREIONIZATION TECHNIQUE FOR CARBON DIOXIDE TEA LASERS(U) UNITED TECHNOLOGIES RESEARCH CENTER WEST PALM BEACH FL OPTICS... W R KAMINSKI 30 NOV 82 1/2

UNCLASSIFIED UTRC/82R-980701-02 DAAK70-81-C-0077 F/G 20/5 NL

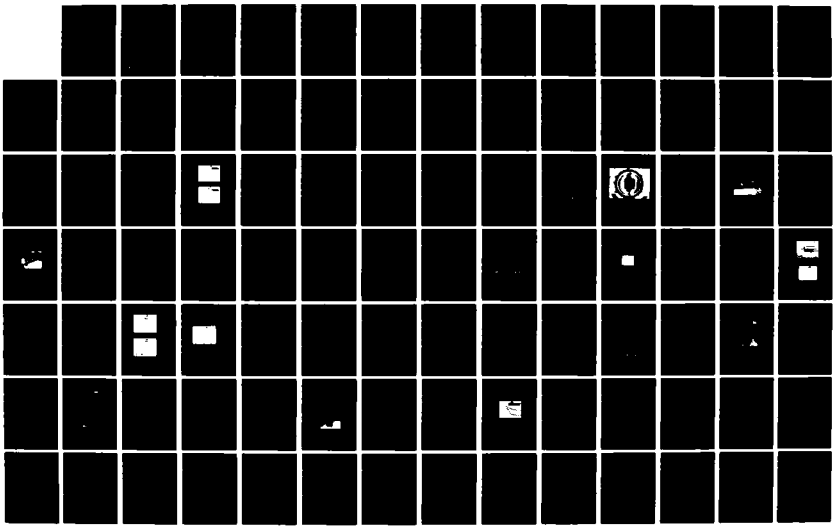

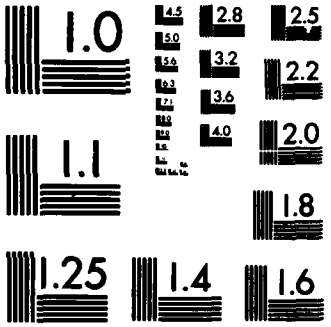

MICROCOPY RESOLUTION TEST CHART
NATIONAL BUREAU OF STANDARDS-1963-A

(12)

82R-980701-02

AD A122552

CORONA PREIONIZATION TECHNIQUE FOR CARBON DIOXIDE TEA LASERS

Walter R. Kaminski

United Technologies Research Center
Optics and Applied Technology Laboratory
P.O. Drawer 4181
West Palm Beach, Florida 33402

November 30, 1982

Final Report

Prepared for:

NIGHT VISION AND ELECTRO-OPTICS LABORATORY
Ft. Belvoir, Virginia 22060

DTIC FILE COPY

DTIC
ELECTE
DEC 16 1982
S D
E

This document has been approved for public release and sale; its distribution is unlimited.

82 12 16 088

SECURITY CLASSIFICATION OF THIS PAGE (When Data Entered)

REPORT DOCUMENTATION PAGE

READ INSTRUCTIONS BEFORE COMPLETING FORM

1. REPORT NUMBER

2. GOVT ACCESSION NO. AD-A122552

3. RECIPIENT'S CATALOG NUMBER

4. TITLE (and Subtitle)
CORONA PREIONIZATION TECHNIQUE FOR CARBON DIOXIDE TEA LASERS

5. TYPE OF REPORT & PERIOD COVERED
Final Report
May 5, 1981 - December 31, 1981

6. PERFORMING ORG. REPORT NUMBER

7. AUTHOR(s)
WALTER R. KAMINSKI

8. CONTRACT OR GRANT NUMBER(s)
DAAK70-81-C-0077

9. PERFORMING ORGANIZATION NAME AND ADDRESS
United Technologies Research Center
Optics and Applied Technology Laboratory
West Plam Beach, Florida 33402

10. PROGRAM ELEMENT, PROJECT, TASK AREA & WORK UNIT NUMBERS

11. CONTROLLING OFFICE NAME AND ADDRESS
U.S. Army Electronics Research & Development Command
Night Vision & Electro-Optics Laboratory (NVEOL)
Fort Belvoir, Virginia 22060 Attn: DELNV-L

12. REPORT DATE
November 30, 1982

13. NUMBER OF PAGES
103

14. MONITORING AGENCY NAME & ADDRESS (if different from Controlling Office)

15. SECURITY CLASS. (of this report)
Unclassified

15a. DECLASSIFICATION/DOWNGRADING SCHEDULE

16. DISTRIBUTION STATEMENT (of this Report)
Approved for public release; distribution unlimited

17. DISTRIBUTION STATEMENT (of the abstract entered in Block 20, if different from Report)

18. SUPPLEMENTARY NOTES

19. KEY WORDS (Continue on reverse side if necessary and identify by block number)

Ultra-Violet Preionization
UV Preionization
Corona Preionization
CO_2 TEA Laser
Laser
Pulsed CO_2 Laser

20. ABSTRACT (Continue on reverse side if necessary and identify by block number)

An experimental program is reported which investigates the basic physics underlying the surface corona preionization process in CO_2 TEA lasers. Measurements were made of UV emission spectra, photoelectron density, current and voltage waveforms and laser output for a matrix of physical parameters known to influence corona preionization. Based upon experimental results, guidelines are given for the design of a corona preionized CO_2 TEA laser.

DD FORM 1 JAN 73 1473 EDITION OF 1 NOV 65 IS OBSOLETE
S/N 0102-LF-014-6601

SECURITY CLASSIFICATION OF THIS PAGE (When Data Entered)

FOREWORD

This final technical report documents research performed from May 5, 1981 to December 31, 1981 under USAMERADCOM Contract DAAK70-81C-0077. The research program was conducted at the United Technologies Research Center (UTRC), Optics and Applied Technology Laboratory (OATL), West Palm Beach, Florida 33408. Dr. Walter R. Kaminski served as the principal investigator and Mr. David N. Spector of the Night Vision and Electro-Optics Laboratory Laser Division, served as the contract technical monitor.

The subject contract was terminated before the technical effort was completed, therefore, all of the technical objectives were not achieved.

Accession For
NTIS CRA&I ☒
DTIC TAB ☐
Unannounced ☐
Justification
By
Distribution/
Availability Codes
Dist | Avail and/or Special
A

DTIC COPY INSPECTED 2

ACKNOWLEDGEMENTS

The author wishes to thank Stan Scalise, Chuck Phaneuf and Eric Koshman of the Optics and Applied Technology Laboratory for all of their assistance. The author also wishes to thank Bill Nighan of the United Technologies Research Center, East Hartford for his useful consultation as well as the interest and encouragement provided by Woodie Fox and Dave Spector of the U.S. Army Night Vision and Electro-Optics Laboratory.

TABLE OF CONTENTS

		Page
	LIST OF FIGURES	iv
	LIST OF TABLES	viii
1.0	SUMMARY	1
2.0	INTRODUCTION	5
3.0	CORONA DISCHARGE UV PREIONIZATION	8
	Background	8
	Corona Preionization Mechanism	9
	Preionization of CO TEA Lasers	16
4.0	DESCRIPTION OF EXPERIMENTAL INVESTIGATION	23
	Corona Discharge Experiment	23
	Laser Preionization Measurement	30
	Laser Output Measurement	34
5.0	EXPERIMENTAL RESULTS	37
	Survey of Operating Conditions	37
	Laser Preioinization Measurement	66
	Laser Output Measurement	68
6.0	CONCLUSIONS AND RECOMMENDATIONS	78
7.0	REFERENCES	80
8.0	APPENDICES	82
	Appendix A - Photoionization of Pulsed TEA Lasers	82
	Appendix B - Design of Experimental Apparatus	93
	Appendix C - Dielectric Microwave Antenna	99

LIST OF ILLUSTRATIONS

		PAGE
Figure 1.	Techniques for producing corona preionization	7
2.	Growth of positive streamer.	11
3.	Growth of negative streamer.	11
4.	Corona preionized laser employing the high voltage gradient technique to generate UV-radiation.	17
5.	Pictorial representation of physical processes involved in high voltage gradient technique of producing a corona.	19
6.	Current waveforms. (a) 20 mega Hz filtered, (b) unfiltered.	20
7.	Optical configuration for detection of ultra-violet emission spectrum.	25
8.	Schematic of corona chamber.	26
9.	View looking into corona chamber. Dielectric plate and electrodes are attached to MACOR carrier and are clearly visible.	27
10.	Laboratory set-up for corona discharge experiment	29
11.	Plexiglass TEA laser with end flanges (for accessibility) used in experimental investigation.	31
12.	TEA laser mounted to monochromator.	32
13.	Schematic diagram of microwave interferometer.	33
14.	Dielectric antennae used to interface between microwave interferometer and laser cavity.	35

15.	Laser output measurement configuration	36
16.	Normal corona glow surface discharge on dielectric plate.	38
17.	Unstable surface discharge which accompanied "Buzzing" sound.	38
18.	Surface spark discharge on dielectric plate.	39
19.	Helium at (a) 1.67 atm., 13.0 KV, (b) 1.0 atm., 13.0 KV.	39
20.	Corona discharge glow over dielectric plate as recorded photographically.	41
21.	Oscilloscope traces of anode voltage (V_A), current (I) and photomultiplier tube outlet (PM) signals for conditions producing surface sparking in test no. 2.20.	44
22.	Corona discharge electrical (current and voltage) and optical signals at λ = 1750 Å.	44
23.	Schematic of experiment to measure charge decay on dielectric plate.	46
24.	Anode voltage and discharge current. (Test no. 2.15).	47
25.	Variation of anode voltage, probe voltage (center location) and discharge current for first 450 n-seconds (Test no. 2.15).	47
26.	Decay of anode voltage and probe voltage (center location) (Test no. 2.15).	48
27.	Corona emission spectrum for individual primary laser gases.	55

28. Corona emission spectrum for two typical laser gas mixtures. 57

29. Comparison of light emission spectrum for three pressure levels of a $He/CO_2/N_2$: 65.0/22.8/12.2 gas pressure. Anode voltage is 17.0 KV. A 1.0 mm MACOR dielectric plate was used. 58

30. Comparison of light emission spectrum for three thicknesses of corona dielectric for a $He/CO_2/N_2$: 65.0/22.8/12.2 gas mixture at 1 atm and an anode voltage of 17.0 KV. 60

31. Comparison of light emission spectrum for three thicknesses of corona dielectric for pure N_2 gas at 1 atm and as anode voltage of 19.0 KV. 61

32. Comparison of light emision spectrum for three electrode gaps for a 2.0 mm thick MACOR dielectric plate. Gas mixture is $He/CO_2/N_2$: 65.0/22.8/12.2 at 1 atm and anode voltage of 10.0 KV. 64

33. Comparison of light emission spectrum for 2 different corona dielectric materials, 2 mm thick. Gas mixture is $He/CO_2/N_2$: 65.0/22.8/12.2 at 1 atm and anode voltage of 10.0 KV. 65

34. Current and voltage waveforms from CO_2 TEA laser discharges. 67

35. Electron density derived from (V)t, I(t) and electron drift velocity. A 1.0 atm mixture of 10% CO_2, 10% N_2 and 8% He was used. 69

36. Pulse energy variation for different corona plate thicknesses. 74

37.	Peak power variation for different corona plate thicknesses.	75
38.	Peak main discharge current for different corona plate thicknesses.	76
A-1.	Streameer breakdown initiated by a single primary avalanche: (a) initial, (b) final charge distributions.	85
A-2.	Preionized breakdown initiated by multiple primary avalances: (a) initial, (b final charge distributions.	89
B-1.	Layout drawing of corona discharge experimental aparatus.	94
B-2.	Electrical circuit components and EMI shielding of corona chamber.	96
B-3.	Electrical system schematic for corona discharge experiment.	98
C-1.	Geometry for design of dielectric microwave antenna.	100
C-2.	Polystyrene plastic microwave antenna design.	102
C-3.	Directional characteristics of a polystyrene microwave antenna at 10 G-Hz.	103
C-4.	Frequency response of a polystyrene microwave antenna/TEA laser cavity.	103

LIST OF TABLES

		PAGE
Table 1.	Surface discharge parameters.	13
2.	Properties of Candidate Corona dielectric plates.	28
3.	Survey of test conditions that produce surface spark.	42
4.	Test summary for corona discharge experiment.	51
5.	Measured capacitance for the corona dielectric plates used in experiment.	54
6.	Test procedures and measurement parameters common to all corona discharge tests.	54
7.	Summary of electrical parameters from thickness comparison tests for a typical 1.0 Atm laser gas mixture (65% He, 22.8% CO_2, 12.2% N_2). Anode voltage is 17.0 KV.	62
8.	Summary of electrical parameters from thickness comparison tests for a typical 1.0 Atm pure N_2 gas. Anode voltage is 19.0 KV.	62
9.	CO_2 TEA laser test data sheets.	70
10.	Effect of varying corona plate thickness averaged over range of N_2/CO_2.	73

1.0 SUMMARY

An experimental program was conducted to investigate the basic physics underlying the surface corona preionization process in a CO_2 TEA laser so that ultimately an optimized laser design can be achieved. Three experiments were planned in order to obtain the necessary data to satisfy program goals. The first experiment focused on the mechanism of corona discharge and the subsequent UV photon emission. The second experiment studied the effects of corona discharge on the initial photoelectron production in the electrode gap and the evolution of the glow discharge that results. The third experiment studied the inter-relationship between UV preionization and laser output by simultaneously measuring those parameters.

As an overview of the experimental program, the following outline is provided.

1. Corona Discharge Experiment
   a. Experimental setup: monochromator fitted with a corona chamber and UV detector.
   b. Measurements: UV photon emission (wavelength vs. intensity) and current and voltage waveforms.
   c. Parameters: 2 dielectric materials, 3 dielectric thickness, 3 dielectric lengths, 3 pressure levels, 6 gas compositions and 4 voltage levels.
   d. Number of test points: 41.
2. Laser Preionization Measurement Experiments
   a. Experimental setup: monochromator fitted with a pulsed CO_2 TEA laser (no optics) and UV detector. Microwave radiation introduced into laser cavity for interferometric measurement.
   b. Measurements: UV radiation, electron density, and current and voltage waveform.

c. Parameters: Same as for corona discharge experiment.

d. Number of test points: 8.

3. Laser Output Measurement Experiment

a. Experimental setup: monochromator fitted with a pulsed CO_2 TEA laser (with optics and UV detector).

b. Measurements: laser output (peak power, total energy, pulse width), UV radiation and current and voltage waveform.

c. Parameters: Same as for corona discharge experiment.

d. Number of test points: 31.

The first part of the corona discharge experiment involved a visual and photographic study to determine gas compositions, voltages, and pressures that produce surface corona discharges. The second part of this experiment dealt with studying the voltage and current characteristics of the preionizer as well the measurement of the spectral response of the ultraviolet corona discharge. Five series of tests were conducted which represent changes in physical parameters known to effect the corona discharge.

In the gas composition tests, it was found that nitrogen is primarily responsible for the UV photon production and CO_2 is the primary absorber of UV photons. Transmission windows were found to exist in an 100 Å wavelength band centered at 1200 Å and for wavelengths above 1600 Å.

In the remaining tests, it was found that the UV light intensity increased when the pressure was decreased from 2.0 atm to 1.0 atm for typical laser gas mixtures. The intensity also increased when the dielectric thickness was reduced or the electrode gap was decreased. UV light intensity was found to increase when the higher dielectric constant material, ZERODUR, was employed. The time rate of change of current is primarily responsible for the light output. This parameter is related to the energy deposited into the plasma. The greater dI/dt the more intense is the UV light output as borne out by the experiments.

In the laser preionization experiment, eight tests were performed using an x-band microwave interferometer to measure preionization electron density. During testing, it was found that preionization electron density could not be measured because of a large noise spike accompanying the voltage switching transient. Considerable effort was expended to minimize the amplitude of the noise signal but to no avail. Electron densities in the main gap were measured by using voltage, current and calculated drift velocity to obtain between 5×10^{13} to 1.1×10^{14} electrons/cc for the various laser gas compositions of interest.

A test series of 30 tests were performed to determine the effect of changes of corona dielectric thickness on laser output and electrical characteristics with all other parameters held fixed. The laser was not attached to the monochromator for these tests because it was being utilized for the corona discharge experiment being performed concurrently.

MACOR was the dielectric material employed having three thickness values of 1.0, 2.0 and 3.0 mm. The anode voltage was kept constant and the gas

composition was varied while mainintaing a 1 atm total pressure. The major result for this test series was that optical pulse energy and peak power increased as the corona plate thickness was reduced. For the 1.0 mm thick dielectric, the pulse energy was 56 mJ, for the 2.0 mm thickness it was 51 mJ and for the 3.0 mm thickness it was 40mJ.

2.0 INTRODUCTION

Carbon dioxide TEA lasers designed for Army rangefinder and target designator applications have unique and challenging requirements. These volume efficient lasers are designed to maximize optical peak power while minimizing pulse widths and rise times. Typically, optical pulse widths are from 60-70 n-sec with rise times less than 25 n-sec. The shape of the optical pulse is also important. Pulses with a minimum tail and a spike having at least 50 percent of the total energy is desirable. In addition, the laser and associated components are often required to survive a rugged operational environment such as that projected for the M-1 tank. However, the most challenging requirement for this laser is long sealed-off operation ($> 2 \times 10^6$ shots) with a shelf life of 5-10 years.

Successful development of a CO_2 TEA laser meeting the above criteria requires that all subsystems be carefully designed. Without minimizing the importance of the other subsystems, the preionizer is of utmost importance from the standpoint of obtaining optimized laser performance and long sealed-off lifetime. Preionization is the necessary means of providing initiating electrons in the main electrode gap such that glow discharge conditions can be maintained consistantly over a wide operating range of conditions. A number of preionization techniques have been developed over the years, but the most applicable technique for small lasers involves the generation of ultraviolet radiation to photoionize the gas volume contained between the main electrodes. Preionizing ultraviolet radiation can be generated by a number of techniques. Some of these include trigger wires, spark discharges, UV lamps, radioactive sources, and coronas.

Corona preionization has recently surfaced as a most promising technique based upon experimental results obtained at OATL and elsewhere. Two basic means of producing corona preionization have been identified. The first involves the use of a suitable dielectric sheet subjected to a high voltage gradient across its thickness at one end. This method was pioneered by Earnst and Boer.[1,2] The second method developed by Hasson, Von Bergman, et al. [3,4,5,6] involves the use of two knife edges separated by a gap with a dielectric sheet backing. These techniques are illustrated in Figs. 1(a) and 1(b). This report covers the first technique which is referred to as the high voltage gradient technique.

The major objective of this research program is to obtain an understanding of the basic physics underlying the corona discharge preionization technique so that an optimized laser design can be achieved. Specific goals for this program are:

1. Measure UV emission spectra, photoelectron density, current and voltage waveforms, and laser output for a matrix of physical parameter changes which are known to influence corona preionization.

2. Study and correlate resulting test data so that the physical processes can be identified and a theory postulated.

3. Produce design guidelines for a corona preionized, pulsed CO_2 TEA laser.

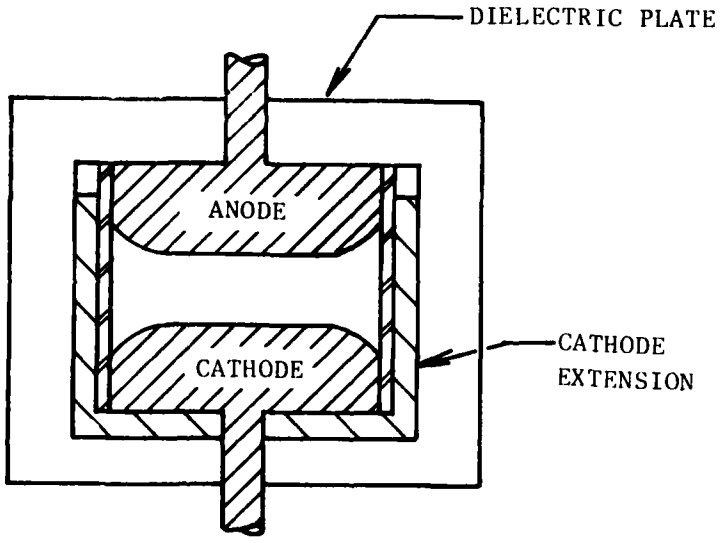

(a) HIGH VOLTAGE GRADIENT

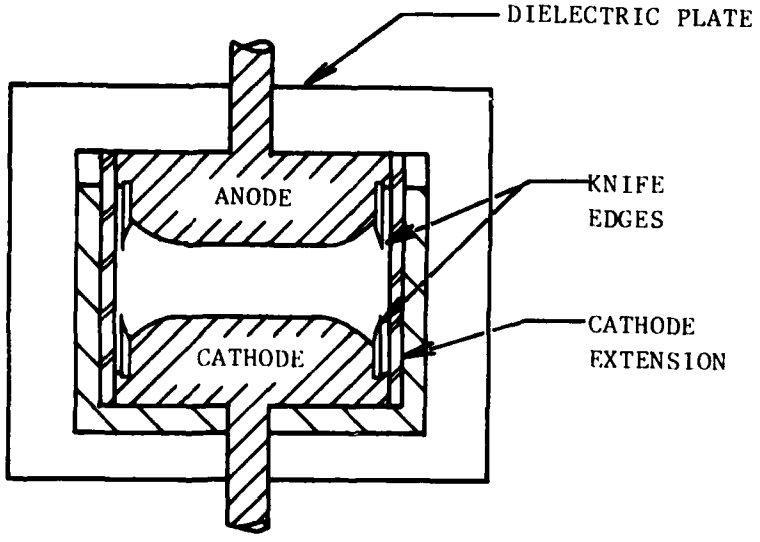

(b) KNIFE EDGE

Figure 1. Techniques for producing corona preionization.

820806017

3.0 CORONA DISCHARGE UV PREIONIZATION

Background

As mentioned in the Introduction, corona discharge is a very effective source of UV preionization, supplying initiating electrons to an electrode gap. This technique of preconditioning has been known for a long time. Meek and Scraggs[7] give reference to work by Wynn-Williams (dated 1926) relating to corona preionization. He showed that the voltage required to cause breakdown was reduced appreciably by a nearby corona discharge. Also consistency of behavior of the gap operation was greatly improved. It was also established that the influence of the corona discharge could be attributed to the light emitted and not to the passage of ions from the corona discharge into the main gap. Meek and Scraggs[7] also referenced work by Berkey (dated 1940) who studied impulse breakdown of a discharge gap in which the electrodes were separated by solid insulating (procelain) spacers. The gap breakdown was found to be appreciably affected by the corona discharges occurring at the boundaries of the insulator and the electrodes. Using rutile (titanium oxide), gave further improvement because it has a higher dielectric constant, of about 80 as compared with a value of about 5 for porcelain. Greater electric gradients were, therefore, produced in the gas near the contacts between the insulating ring and the electrodes when rutile was used, and surface corona discharges were therefore enhanced, with consequent improvement in the impulse characteristics of the main gap.

From an historical standpoint, it appears that the corona preionization technique was put aside in favor of spark discharge preionization by the early investigators. Because the spark discharge technique was well understood, it was favored by designers of high voltage electrical equipment and subsequently by the early pulsed CO_2 TEA laser investigators. Only recently[1,2,3,4,5,6] has the corona discharge been applied as the

preionization source for pulsed CO_2 TEA lasers. If one examines these early references, one observes that primarily two groups have been developing this technology. The group from Pretoria, South Africa has developed what was referred to in the Introduction as the knife-edge technique (Fig. 1a). The high voltage gradient technique was pioneered by researchers from Twente University, The Netherlands (Fig. 1b).

The potential of the high voltage gradient technique, as a means of providing UV preionization for a CO_2 TEA laser, was recognized early in our research activity. Work was initiated on developing this technology in December 1979, shortly after discovering the literature sources[1 2]. Although the knife-edge technique is also a viable means, we feel that the high voltage gradient technique lends itself to long sealed-off lifetime for reasons which will be made clear later in this section. However, a complete understanding of the basic physics involved in both of the methods is lacking. For this reason, the subject research program was undertaken in an effort to gain an understanding of the fundamentals involved in this preionization scheme so that it could be fully exploited in future designs.

Corona Preionization Mechanism

This section presents a limited discussion concerning the phenomena of corona discharges and applies to both of the above identified corona preionization schemes. Additional information can be found in Hirsch and Oskam's[8] excellent text.

The term "corona discharge" refers to a phenomena which occurs in a gaseous medium in the vicinity of conductors of small radius of curvature, subjected to intense, but not disruptive, electric fields. Recent studies have shown that the corona discharge rightfully belongs to the general class of glow discharges. However, there is a fundamental difference between a corona discharge and a discharge which occurs in an electrode gap as discussed further in this section.

When an electrode gap is subjected to a uniform electric field and initiating electrons are introduced into the gap, breakdown occurs. In the case of a corona discharge, both the electric field and consequently the Townsend α (first ionization coefficient) are functions of position in space.
In the non-uniform electric field case, partial-breakdown can occur and the processes can take place long before complete voltage breakdown between the electrodes takes place.

Two basic types of coronas exist. They are related to which of the electrodes is stressed (i.e., the electrode having the nonuniform electric field). The polarity of the stressed electrode determines the direction of the potential gradient and the flow of the charged particles. The basic physical difference between the anode corona and the cathode corona is in the way that the avalanches grow between the electrodes. Sketches illustrating the proposed mechanisms are given in Figs. 2 and 3. In the case of of the positive streamer, or cathode directed streamer, shown in Fig. 2, photons are thought to produce photoelectrons ahead of the streamer and these initiate avalanches which develop towards the tip of the streamer because of the attraction of the positive space-charge field surrounding the tip. Each successive incoming avalanche causes an extension of the streamer, as illustrated in Fig. 3, and it grows as the result of successive avalanches developing away from the streamer tip in the space-charge field surrounding the tip. There avalanches may be initated by electrons from the tip or by photoelectrons produced in the gas ahead of the tip.

The mechanism for self-sustained streamers for a corona is very similar to the mechanism presented in Appendix A for glow discharge in a uniform field gap. The major difference is that here the coefficeint of ionization by electron collision, that is, the magnitude of Townsend's α, has to rely more on local field augmentation by positive-ion concentration of previous avalanches. Meek and Scraggs[7] gives an

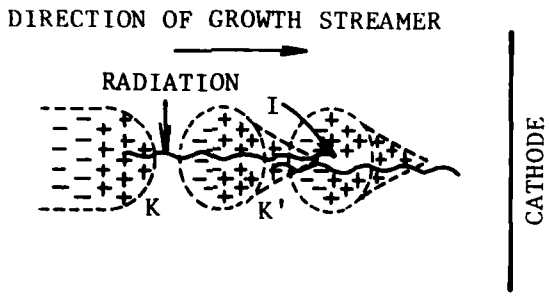

Figure 2. Growth of positive streamer.

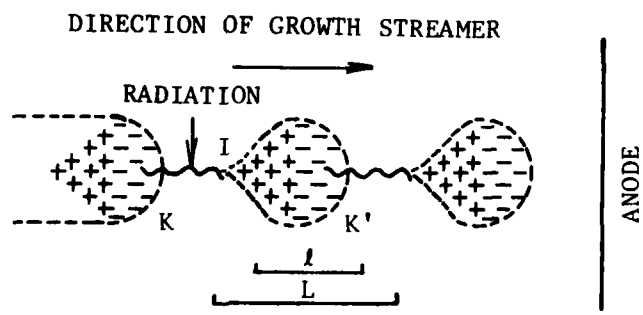

Figure 3. Growth of negative streamer.

expression for self-sustained streamers which was originally presented by Pedersen (Ref. 37 in Meek and Scraggs). Pedersen assumes that a streamer leading to breakdown develops when the density of positive ions at the head of the avalanche attains a certain value, and on this basis has formulated the breakdown condition

$$\log_e \alpha_x + \int_0^x \alpha \, dx = g\,(x,p) \qquad (1)$$

where α_x is the value of α at the head of the avalanche and $g(x,p)$ is a function of x and gas pressure which depends upon the field distribution. Note the similarity of Eq. (1) with Eq. (A-6) as presented in Appendix A.

Thus far, the discussion has centered upon how a corona is initiated and how it develops into a self sustained discharge. It is appropriate now to discuss the varius regimes that can exist after a surface discharge becomes self sustaining. The discussion will also include the light emission properties of these discharges.

An excellent article was written by R. E. Beverly, III[9] which discusses light emission from high current surface spark discharges. Beverly defines parameters, given in Table 1, which govern surface discharges.

TABLE 1. SURFACE DISCHARGE PARAMETERS

Electrical:	Capacitance of the energy-storage capacitor, C Circuit inductance, L Charging voltage, V_c Electrical circuit efficiency, η_{el}
Mechanical:	Substrate composition Electrode composition Source geometry Surface gap, l
Environmental:	Gas composition Gas pressure, P

The ratio, V_c/L, has been defined by Beverly as the "hardness" or "strength" of a discharge. This parameter imposes an upper limit for the initial rate of change of the current with time and largely determines the initial rate of energy input into the discharge channel and hence its light emission characteristics. Note that for a low inductance driving circuit,

$$\left(\frac{di}{dt}\right)_{max} = Vc/L. \qquad (2)$$

Beverly defines two regimes based upon the parameter V_c/L. For $V_c/L \leq 10^8$ Volts/Henry, the discharge is considered weak whereas for $V_c/L > 10^{10}$ V/H the discharge is very strong in terms of current and light emission. In the strong discharge regime, radiation emitted by the plasma heats and vaporizes surface constituents which modify the gas-dynamic and radiative behavior. In fact several examples are given where a dielectric is chosen based upon the wavelength desired from the discharge. For the high current regime,

erosion due to radiative vaporization of the substrate material ultimately limits the life expectancy of the source. Another problem that is encountered in this regime of operation is that sputtered material from the electrodes is transported into the discharge channel and can partially condense on the dielectric substrate following the discharge. For these reasons, the weak discharge regime is the preferred regime to operate the CO_2 TEA laser having a 2×10^6 pulse sealed-off lifetime requirement.

In the weak surface discharge regime (coronas) the dielectric material affects the light source in the following manner. The dielectric strength of the material determines the thickness that is required to hold off the voltage gradient. The thickness, d, in turn determines the interelectrode surface capacitance, C_s. For the simple case of a dielectric bonded to a rear surface ground plane C_s is given by equation (3).

$$C_s = \varepsilon/d \qquad (3)$$

C_s is in pF/cm^2 and $\varepsilon = \kappa\varepsilon_o$ is the dielectric permittivity, κ is the dielectric constant and ε_o is the permittivity of free space. The normal field component E_n (volts/cm) is related to the surface charge density, σ_s, which is in turn related to the voltage, V, and surface capacitance by the following relationship,

$$E_n = 4\pi\sigma_s = 4\pi V C_s. \qquad (4)$$

Hence, lower breakdown voltages will be obtained for thin dielectic plate thicknesses having large dielectric constants. The dielectric plate thickness and permittivity or dielectric constant also determines the current flowing between electrodes. Equation (5) shows that the displacement current i_d is a function of the dielectric's capacitance and the rate of change of voltage with respect to a change in time. It should be noted that i_d

$$i_d = C_s \, dV/dt \qquad (5)$$

is not the total current flowing through the discharge. A plasma current i_p is also present when the surface discharge reaches breakdown. Thus, total current is given by (6).

$$i = i_d + i_p \qquad (6)$$

Both Tallman[10] and Baranov, et.al.[11], have experimentally determined that the displacement current is related to the radiative properties of the discharge. The magnitude of the radiative output is also dependent upon the time rate of change of current with time.

Based upon work reviewed by Beverly[9], the radiative emission from a surface discharge is due to three mechanisms; namely, electron-ion free-free transitions (Bremsstrahlung continuum), overlapping free-bound transitions (recombination continuum) and bound-bound transitions (atomic and ionic lines). For weak discharges, $V_c/L \leq 10^8$ V/H, a weak continuum and a few lines of excited gas are typically observed. The lines are not highly broadened and are easily identifiable against the continuum. As the discharge strength increases, more line transitions are excited and becomes increasingly broad as the result of the Stark effect. For very strong discharges, typically $V_c/L > 10^{10}$ V/H, the visible and near-ir emission becomes nearly continuous in apperance for various gases at high pressure. In the ultraviolet, significant differences in the emission characteristics exist between the various gases, even for strong discharges at pressures of several atmospheres. Another important point to note is that for a given V_c/L, the radiant intensity peaks at approximately the same time as the maximum in current occurs for a heavy gas while for lighter gases such as H_e, the peak optical intensity occurs later. This behavior is important to keep in mind when trying to maximize the laser optical output by minimizing the timing between the preionization current pulse peak and electrode gap current peak.

Preionization of CO_2 Lasers

Configuration

Figure 4 shows the essential features of a laser employing the high voltage gradient technique for generating the UV radiation which is used to preionize the electrode gap. The hardware components are housed in a dielectric chamber structure. At this time MACOR (a machinable glass ceramic) is the material of construction because of its excellent electrical properties (dielectric constant = 5.9 and dielectric strength = 1000-3000 V/mil). MACOR is also virtually impervious to Helium absorption, permeation rate = 4.2×10^{-12} (cc(stp)-mm/sec cm^2 - cmHg), and does not contain any substances which can outgas after proper bakeout. Porosity for this material is zero. The electrodes are fabricated from either aluminum or nickel and are profiled according to design procedures given by Chang[12]. The Chang parameters used are k = .02, u = arc cos (-k) and a 1.0 cm gap. An extra 0.500 cm was added to the basic electrode thickness to provide material for fastening the electrical feedthrough screws. A copper U-shaped cathode extension is used to produce the high electric gradient across the thickness of the upper portion of the dielectric (across from the anode). MACOR is often used as the dielectric side plate material. Typically, a dielectric plate thickness is 2.00 mm is used although there are advantages to using thinner plates as will be discussed further in this report.

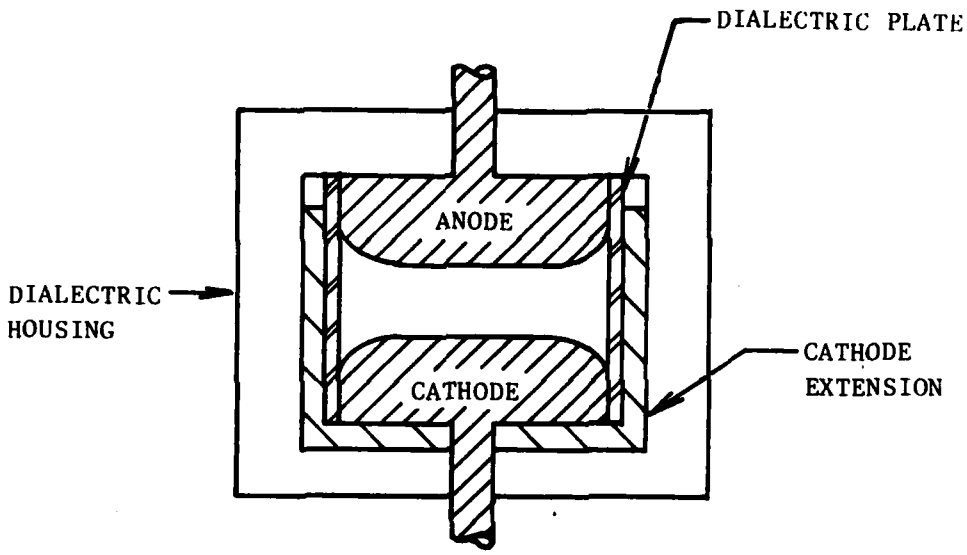

Figure 4. Corona preionized laser employing the high voltage gradient technique to generate UV-radiation.

Principle of Operation

The physical principles involved in producing a surface corona discharge in a laser is explained with the aid of Fig. 5. When the pulser spark gap is fired, a rapid voltage rise appears between the copper plates and the opposite polarity (anode) electrode. A very high electric field with a rapid rise appears between them. We have measured a voltage pulse across the electrodes with a 20 n-sec rise time. The electric field is uniform in the z direction (parallel to the length of the electrode). Since the dielectric plate is subjected to an electric field, it becomes polarized with surface electrons present. The electrons are easily pulled from the dielectric due to the steep electric field in the corner formed by the dielectric and the anode. Once a sufficient number of electrons are present in the gas, streamers form which rapidly develop into avalanches. The streamers are uniform in the z or lengthwise direction by virtue of the uniform electric field. This situation produces a corona discharge having good uniformity. Since the anode is identified as the "stressed electrode," the corona is classified as an anode type corona and the plasma proceeds to travel along the dielectric plate in a direction y, from the cathode to the anode. The resulting plasma which is confined to the vicinity of the dielectric plate forms a channel for the passage of current from the anode to the cathode.

At this point it is worthwhile to examine measured current waveforms (Figs. 6(a) and 6(b). Figure 6(a) shows a filtered (20 mega-Hz) current waveform which is instructive for purposes of obtaining general information. The first current pulse is identified with the preionization process.* The preionization current

---

* During experimentation, the dielectric plates were removed and a pulsed voltage applied. These smaller current pulse disappeared and the main gap arced.

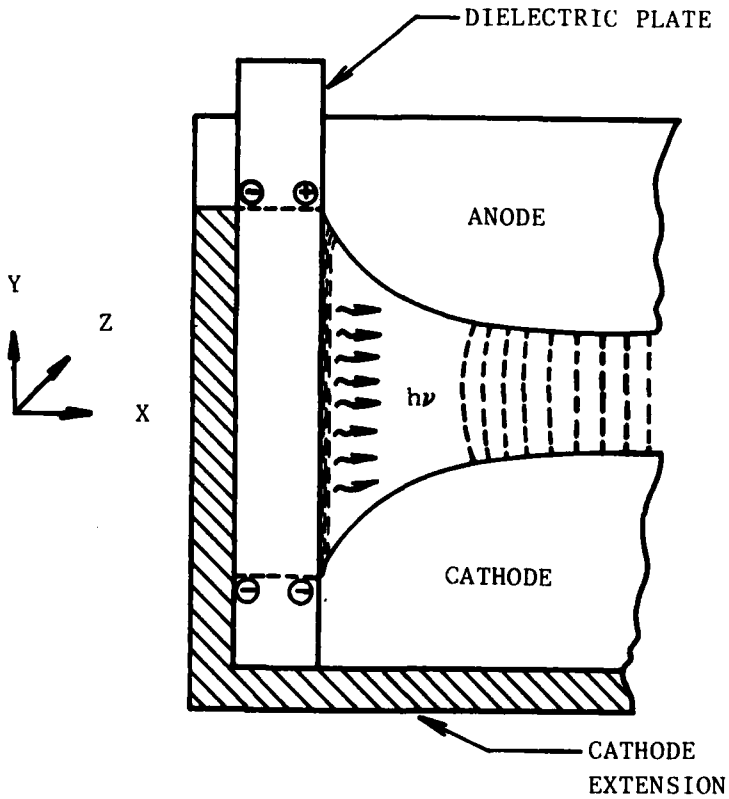

Figure 5. Pictorial representation of physical processes involved in high voltage gradient technique of producing a corona.

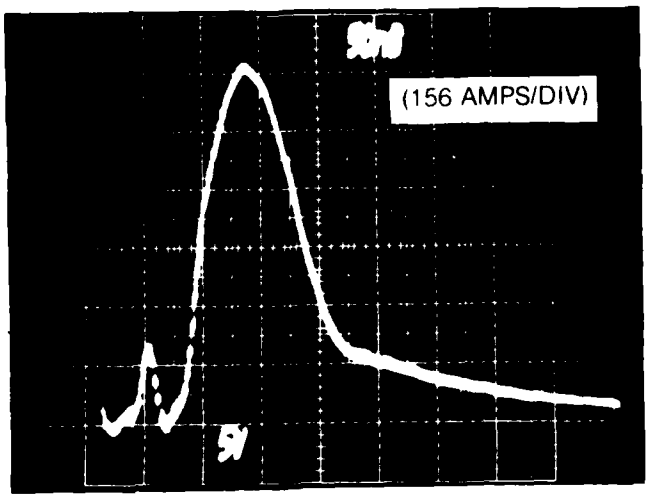

(a)

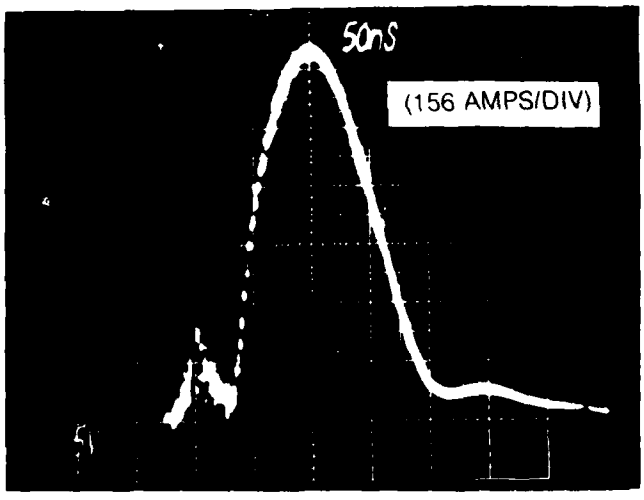

(b)

Figure 6. Current waveforms (a) 20 mega Hz filtered, (b) unfiltered.

82-10-18-3

pulse is approximately 25 n-sec wide with a peak current of 187 amps as compared to the main gap peak current of 952 amps. As discussed in the previous subsection, the preionization current is composed of a displacement current which charges the dielectric and a plasma or corona current as given by equation (6). This topic will be discussed further in the Experimental Results section. Approximately 2-3% of the electrical energy delivered to the electrodes was consumed by the preionization pulse (as determined from $V(t) \cdot I(t)dt$). Figure 6(b) shows an unfiltered current waveform (test conditions were not the same as those for Fig. 6(a). The current signal shows a higher frequency component which is theorized to be related to plasma dynamic conditions. Electrons are lost from the plasma near the dielectric by three processes: (1) loss to the wall as a result of wall collisions, (2) drift of electrons out the volume occupied by the plasma, and (3) attachment to gas molecules as a result of collision processes.

The observed ocillations occur as a result of the distortion of the electostatic field by both positive and negative ions that are present in the region near the dielectric plate. These space charges distort the original field so that a new streamer cannot develop until the previous streamers have dissipated or cleared the region near the dielectric. This condition causes the electron density in the plasma to oscillate and give rise to a temporally oscillatory current as observed.

The UV photons emitted by the corona discharge are symmetrical about a centerline perpendicular to the electrodes and uniformly illuminates the electrode gap. The UV source extends over a region equal to the size of the dielectric plates and is very uniform. This does not preclude a gradient in photon emission in a direction across the width of the plates. This gradient is relatively unimportant. The resulting glow discharge is excellent with no streamers visible. The generated CO_2 laser beam has been observed to be of high optical quality based upon power profiles observed in the far field.

Physical variables which influence the surface corona preionizer are (1) dielectric thickness, (2) dielectric length from anode to cathode, (3) dielectric material, (4) system stray capacitance and inductance (5) voltage pulse rise time, (6) voltage level, (7) pressure, and (8) gas composition.

The advantage of corona discharge preionization as compared with other methods of generating UV preionization are listed below. Several of the advantages are inherent in the production of the uniform, streamerless, glow discharge that forms in the electrode gap. All of the advantages with the exception of (5) apply equally to both the high voltage gradient and knife edge techniques. Operational life is expected to be affected by the sharp knife edges which may be subject to erosion[13]. Furthermore, it is theorized that higher local voltage gradients in the gas around the knife edges may cause a greater amount of CO_2 dissociation than for the voltage gradient technique.

(1) Uniform U-V illumination of the gap region which generates the initiating electrons,

(2) Preionization is accomplished by low energy expenditure,

(3) Single discharge of electrical energy by a single pulser circuit,

(4) Consistant arc-free operation over a wide set of operating conditions,

(5) Compatability with long sealed-off lifetime operation and long shelf life,

(6) Excellent beam quality due to spatially uniform UV preionization.

4.0 DESCRIPTION OF EXPERIMENTAL INVESTIGATION

The purpose of this section is to state the specific objectives of the various planned experiments and to describe the apparatus used. Although contract funding was terminated before all of the planned experiments could be completed, it is felt that documentation is worthwhile in the event that this work would be picked up in the future. Considerable effort was expended in planning and designing these experiments.

Three experiments were planned in order to obtain the necessary data to satisfy the objectives and goals stated in the Introduction. The first experiment focuses on the mechanism of corona discharge and the subsequent UV photon emission. The second experiment studies the effects of corona discharge on the initial photoelectron production in the electrode gap and the evolution of the glow discharge that results. The third experiment studies laser output. For each of these experiments physical variables are systematically investigated.

Corona Discharge Experiment

The purpose of this experiment is to acquire data so that the physics underlying the initiation, growth, and decay of the corona discharge may be studied. Data will be acquired to determine the UV radiation characteristics

in terms of wavelength and intensity. Figure 7 shows the optical configuration for performing the corona discharge experiment. The experimental setup consists of a corona chamber, a vacuum monochromator, and a UV detector (photomultiplier with a sodium salicylate scintillator). This experimental setup is similar to the one used by McKen, et al.[14] The ultra-violet emission spectrum produced by the corona discharge is examined with a vacuum UV monochromator, a McPherson Model 218 scanning monochromator with a 1200 groove per millimeter grating blazed for 1500 Å. With this grating, the monochromator has a 0.6 Å resolution.

The UV photon detector utilized in these investigations is a McPherson Model 650 detector assembly. This detector assembly, which is fitted to the exit port of the monochromator, operates as follows. Ultraviolet radiation leaving the monochromator passes directly to a sodium salicylate coated vacuum-tight window, which upon irradiation, fluoresces. This fluorescent energy (at a wavelength of approximately 4000 Å) passes through an air space, through the window of the photomultiplier envelope and strikes the photocathode surface. The photomultiplier then converts the light energy striking its cathode into an electrical signal that can be amplified and read out on a suitable recorder. The spectral response of this device is flat through a range of 300 to 3000 Å.

The corona chamber shown in Fig. 8 contains a fixture which holds a dielectric plate, anode and cathode electrodes, a pressure tap, inlet and outlet flow ports, and a rear port (with plug) that can be used for initial optical alignment. Fig. 9 shows a photographic view looking into the corona chamber. The fixture holding the dielectric and electrodes can be translated in the vertical direction. The rear port also allows the insertion of a standard spark plug for checking the entire system for operation as needed since the UV radiation characteristics of a spark plug are well known. The corona chamber was designed to have a minimum path length from the dielectric plate to

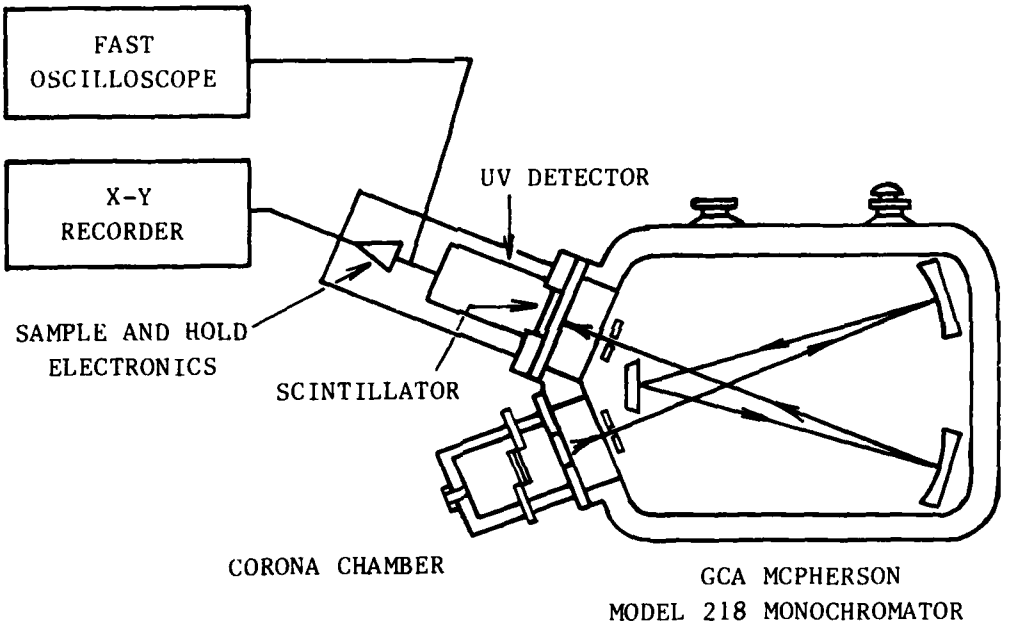

Figure 7. Optical configuration for detection of ultraviolet emission spectrum.

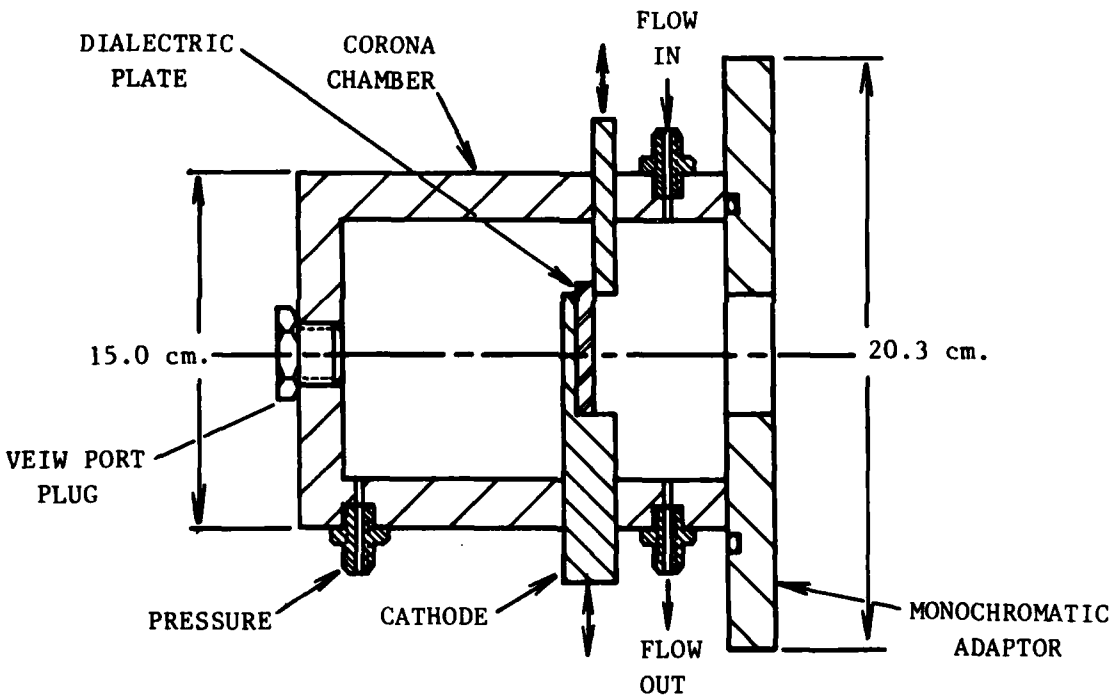

Figure 8. Schematic of corona chamber.

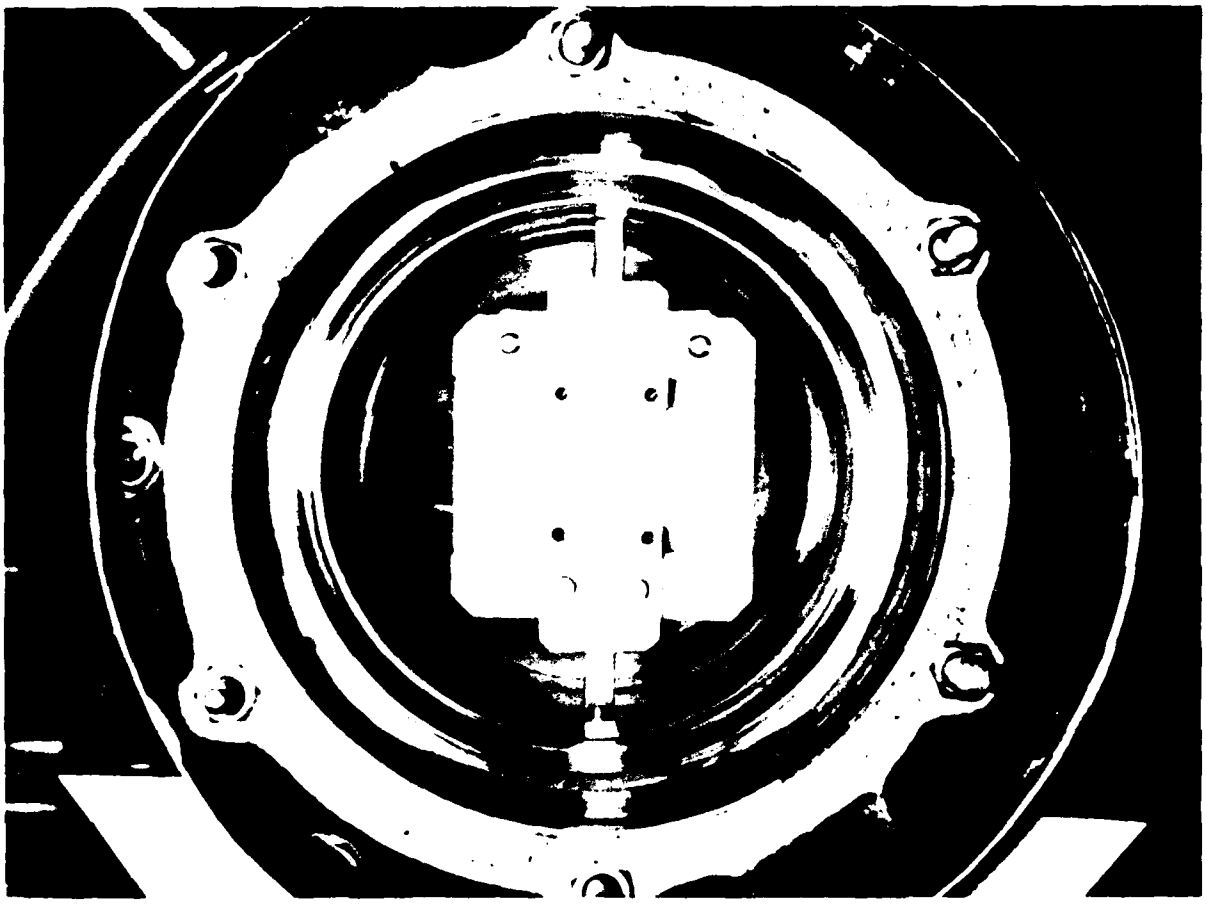

Figure 9. View looking into corona chamber. Dielectric plate and electrodes are attached to MACOR carrier and are clearly visible.

82-10-18-2

the monochromator LiF window in order to minimize absorption of UV radiation. The material of construction used was MACOR^R. Appendix B contains a description of the design details of the experimental appartus.

Electromagnetic shielding was used to minimize RF interference from the high voltage components. Figure 10 shows the complete laboratory setup for this experiment.

The signals from the UV detector are recorded on an X-Y recorder with the monochromator scanner serving as the voltage driver for the X-axis. The monochromator is scanned in wavelength from 1050 to 2000 Å.

In this experiment the following physical parameters were investigated:

(1) Dielectric material: MACOR^R, Pyrex glass and Zerodur^R. See Table 2 for properties of candidate corona dielectric plates.

(2) Dielectric thickness: 3 thicknesses, 1.5, 2.0, and 3.0 mm.

(3) Dielectric length: length over which voltage gradient exists (2.03, 1.65, 1.27 cm)

(4) Pressure level (0.5, 1.5, 2.0 atm).

(5) Gas composition (6 typical laser gas compositions spanning range of He, CO_2 and N_2).

(6) Voltage ramp rate.

TABLE 2. PROPERTIES OF CANDIDATE CORONA DIELECTRIC PLATES

MATERIAL	VOLUME RESISTIVITY (OHM-CM)	DIELECTRIC STRENGTH (V/MIL)	DIELECTRIC CONSTANT	THERMAL EXPANSION (1/DEG.C)	MAX. USEFUL TEMPERATURE (DEG. C)
MACOR^R	10^{14}	3000	5.92	1.1×10^{-5}	1000
PYREX GLASS	10^8-10^{11}	127 - 7600	4.60	$.32 \times 10^{-5}$	700
ZERODUR^R	2×10^{13}	-	7.40	$.005 \times 10^{-5}$	370

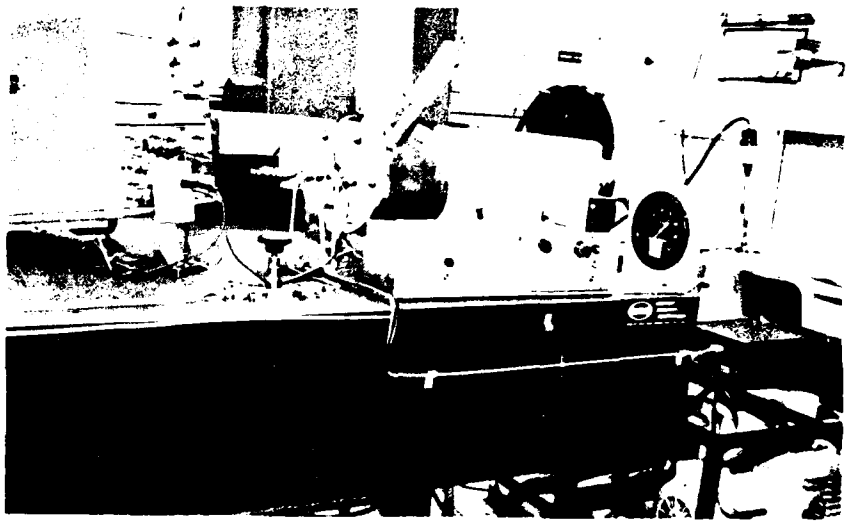

Figure 10. Laboratory set-up for corona discharge experiment.

82-10-18-4

Laser Preionization Measurement Experiment

In this experiment, simultaneous measurements of UV radiation and preionization electron density are made in a pulsed CO_2 TEA laser cavity. The laser shown in Fig. 11 was modified for mounting to the McPherson monochromator as shown in Fig. 12. A slit was made in one of the dielectric side plates to permit UV radiation to enter the monochromator. In this experiment, the laser replaces the corona chamber as shown previously in Fig. 7. Microwave radiation is introduced into the laser cavity through the optic mounts (less optics). By using a microwave interferometer arrangement as shown in Fig. 13, average photoelectron density in the optical cavity can be measured.

Microwave interferometry is a well established diagnostic used in plasma physics.[15] It was successfully applied to measure photoelectron density generated by a spark which served as the UV preionization source for a CO_2 TEA laser.[16] The technique involves the measurement of the phase shift and attentuation introduced to a microwave beam by the presence of a plasma in the cavity. The measurement consists simply of noting the differential phase and attentuation required to rebalance the interferometer in the presence of the generated plasma. Hence, the measurement is a null technique and capable of high accuracy and repeatability, determined mainly by the precision of the interferometer components and signal-to-noise ratio of the detection system.

The microwave interferometer shown schematicaly in Fig. 13 is particularly useful in measurements of transient plasmas. It should be pointed out that a Faraday cage was installed around the laser, high voltage components, pulse electronics and power supplies to isolate E-M signals from interfering with the microwave measurements. An X-band system frequency (8.20 G-Hz to 12.40 G-Hz) was originally selected as a compromise between minimal detectable plasma density (during preionization), size of the laser cavity, and magnitude of the collision frequency expected at the pressures planned for this experiment.

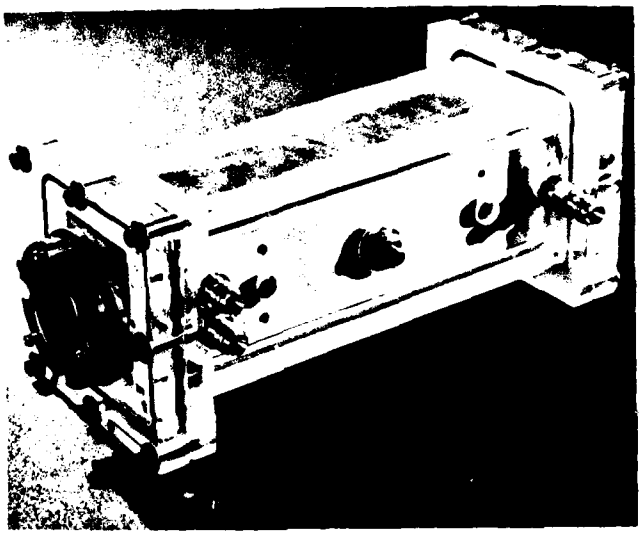

Figure 11. Plexiglass TEA laser with end flanges (for accessibility) used in experimental investigation.

82-10-18-5

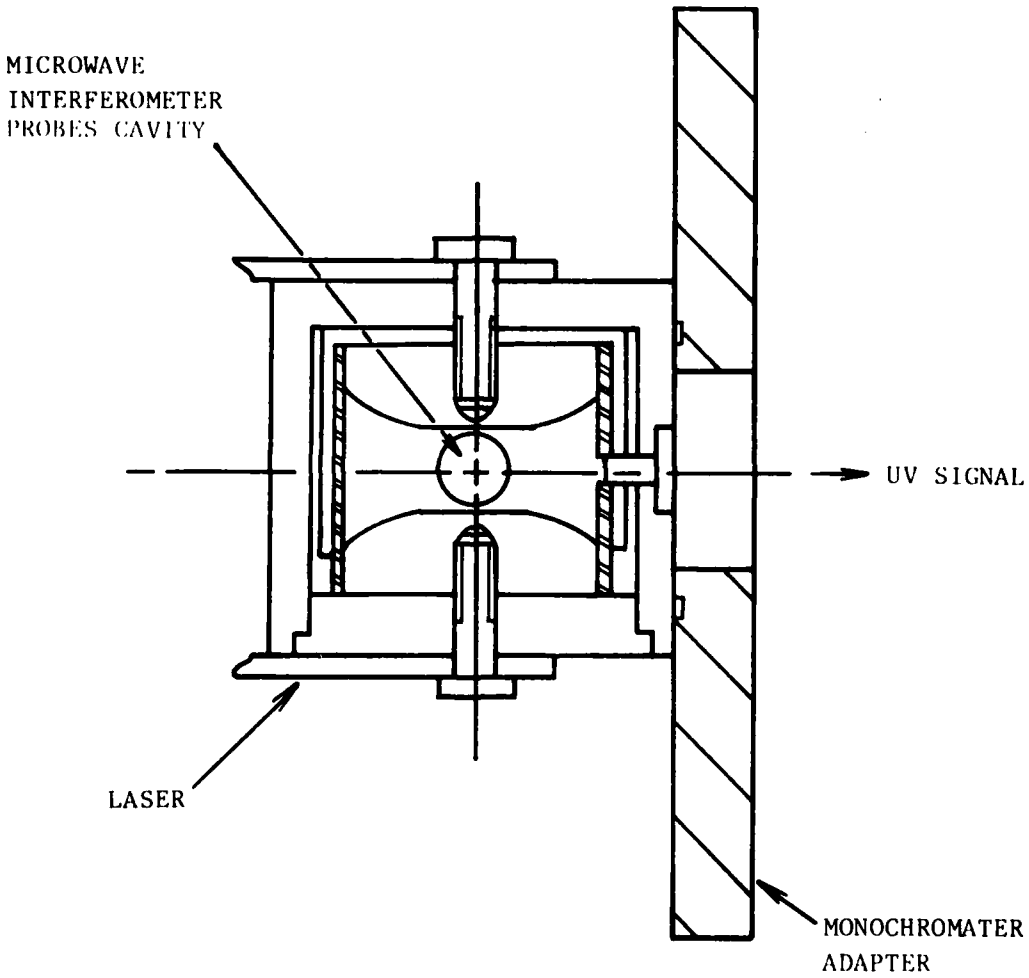

Figure 12. TEA laser mounted to monochromater.

820806023

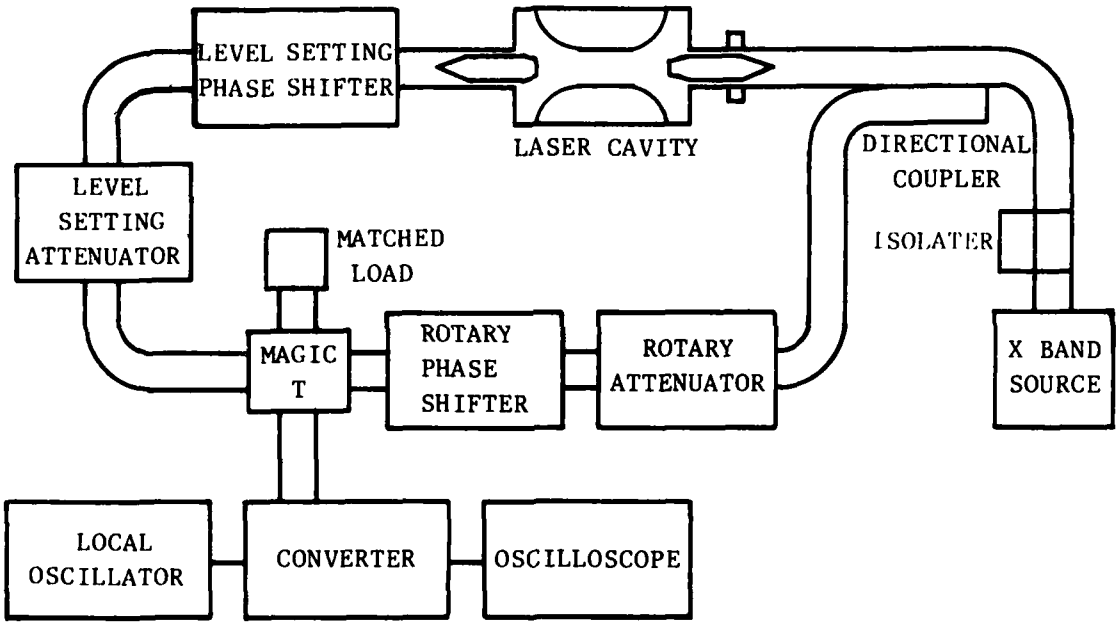

Figure 13. Schematic diagram of microwave interferometer.

This interferometer is capable of electron density measurements of $3x10^7$ to $1.3x10^{12}$ electrons/cc as reported by Seguin[16] which should be sufficient for preionization measurements.

According to Seguin, the measured electron density range was approximately 10^6 to 10^{12} electrons/cc and thought to be typical for CO_2 TEA lasers.

To eliminate large reflection losses at the laser cavity interface with the microwave system, polystyrene rods serving as waveguide antennae were inserted into the laser cavity as shown in Figure 14. The polystyrene waveguides were designed using the internal reflection principle in a manner which maximizes the direction-ability of the launched microwave as discussed in Appendix C. The laser cavity with its metal electrodes propagates microwaves in the same manner as a waveguide.

The same parameters are investigated in this experiment as stated for the corona discharge experiment. Therefore, results from this experiment will give comparison with those from the first experiment.

Laser Output Measurement Experiment

Utilizing the same laser and monochromator setup as for the preionization experiment, laser output and UV radiation will be simultaneously measured. For this experiment, laser optics will be installed and the microwave interferometer will be removed. Specifically, laser peak power, pulse width, total energy, current and voltage waveform, UV intensity and wavelength will be simultaneously measured. The laser output measurement configuration is shown in Fig. 15. By simultaneously measuring laser output and UV radiation, data on how much irradiation is necessary for breakdown and subsequent lasing will be obtained. A time correlation between UV production and lasing when coupled to current and voltage waveforms is important to the understanding of the dynamical behavior of the processes involved. As stated previously, the same parameters will be investigated in this experiment as for the first experiment.

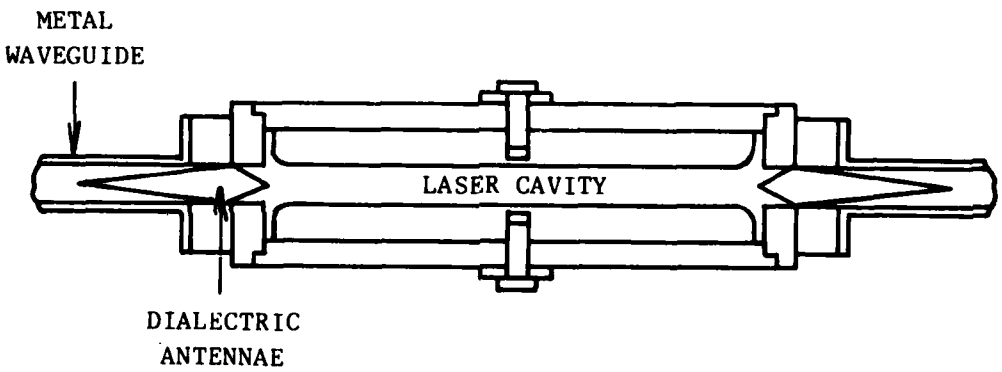

Figure 14. Dialectric antennae used to interface between microwave interferometer and laser cavity.

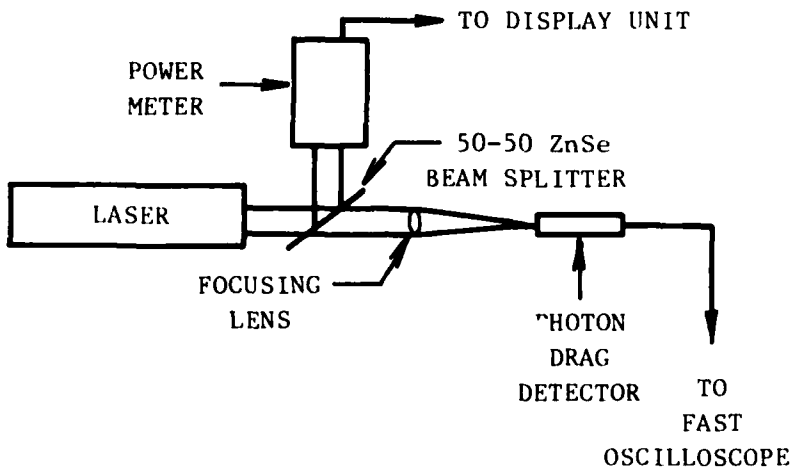

Figure 15. Laser output measurement configuration.

5.0 EXPERIMENTAL RESULTS

Survey of Operating Conditions

The first part of this experiment involved a visual and photographic study to determine the proper voltage levels to be set for the various planned test conditions. It was necessary to operate in the weak surface discharge regime (as discussed in Section 3) which corresponds to conditions in the laser as will be shown. The full range of gas compositions, voltages and pressures were investigated visually for a fixed geometry in these preliminary tests.

Initial tests were performed using a 2mm thick MACOR dielectric plate and an atmospheric pressure $CO_2/N_2/He$: 22.8/12.2/65.0 laser gas mixture. For voltages below 17.0 KV, a uniform purple glow discharge was observed as shown sketched in Fig. 16. This type of discharge is described as a corona in the text which follows. The corona glow was not cloud like but was actually composed of very closely spaced streamers which were judged to be less than a quarter of a millimeter in width. As the voltage was raised to 17.5 - 18.0 KV, a buzzing sound could be heard. The streamers thickened and separated with gaps forming between them. The thicker streamers then tried to propagate from anode to cathode but stopped at 1/3 to 1/2 the distance away and oscillated as shown in Fig. 17. The discharge pattern below the thick streamers was not discernable because their brightness obscurred any other patterns occuring. As the voltage was raised above 18.0 KV to approximately 18.5 KV, a surface spark discharge was observed as sketched in Fig. 18. The surface spark would meander over the 2.54 cm x 2.54 cm field of the dielectric. For voltages above 18.5 KV, the surface spark would become stabilized in location and increased in brightness.

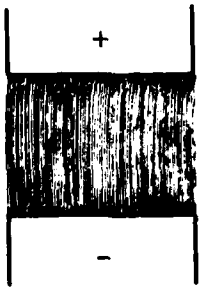

Figure 16. Normal corona glow surface discharge on dielectric plate.

820806013

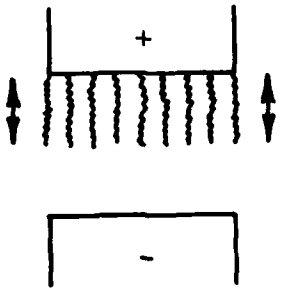

Figure 17. Unstable surface discharge which accompanied "Buzzing" sound.

820806014

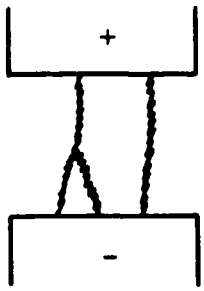

Figure 18. Surface spark discharge on dielectric plate.

820806011

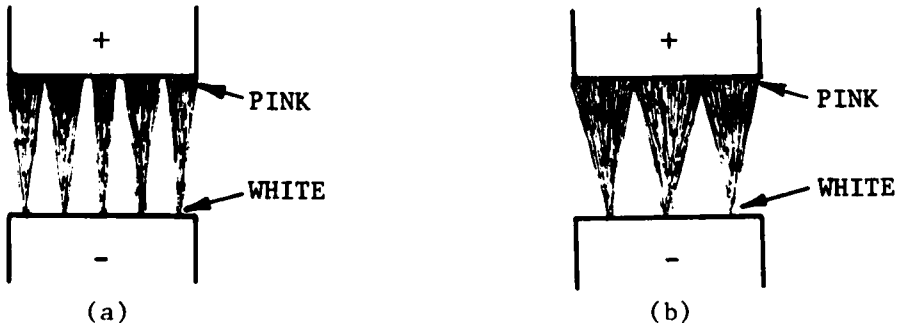

Figure 19. Helium at (a)1.67 atm, 13.0 kv (b)1.0 atm, 13.0 kv.

820806012

Pure helium was then substituted for the laser gas mixture. At 13.0 KV* the patterns appearing in Figs. 19(a) and 19(b) were observed. Five feathery discharge channels with wide gaps appeared as shown in Fig. 19(a) at 1.67 atm. As the pressure was decreased to 1.0 atm, the brightness near the cathode increased and 3 wide feathery discharge channels could be observed as shown in Fig. 19(b). These patterns were much different than those for other gases studied.

An attempt was made to photograph the visible component of the corona discharge. Figure 20 shows a typical corona discharge glow observable over the dielectric plate as recorded photographically using a long exposure time. For this case, the dielectric utilized was a 2 mm MACOR plate with the anode and cathode separated by 2.03 cm. The gas was 95% N_2 and 5% He at 1 atm with an impressed voltage of 22.5 KV. The glow pattern was found to be dependent upon composition, pressure and voltage with varying intensity. The bright glow observable was due to sharp edges on the electrodes which was subsequently eliminated when the edges were rounded off.

This test series concluded with a survey of test conditions that produced surface sparking. Table 3 summarizes those results. As can be observed, pure helium produces surface sparking at very low voltages over the entire pressure range explored. Nitrogen and carbon dioxide (in that order) increase the threshold level of voltage for sparking. As expected, increasing gas pressure raises the voltage required for the sparking condition. The column entitled light pulse delay time refers to the observance of a photomultiplier

---

*This was the lowest setting of power supply at time of experiment but was later modified to permit operation at lower voltages.

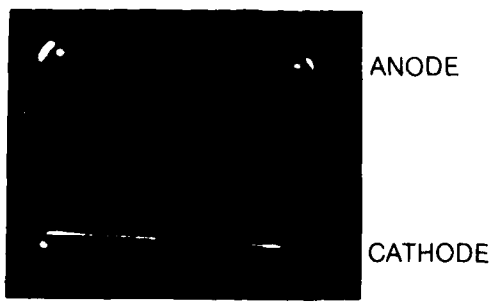

Figure 20. Corona discharge glow over dielectric plate as recorded photographically.

82-10-18-6

TABLE 3. SURVEY OF TEST CONDITIONS THAT PRODUCE SURFACE SPARK

COMPOSITION (%)			PRESS. (ATM)	INCIPIENT VOLTAGE FOR SURF. SPARK (KV)	LIGHT PULSE DELAY TIME (μ-SEC)	COMMENTS
He	CO_2	N_2				
100	0	0	1.00	< 13.0	(1)	Immediate Surface Spark Condition (See Figures 5.4(a) and (b)
			1.33	< 13.0	(1)	
			1.67	< 13.0	(1)	
0	0	100	1.00	21.0	2-8	
			1.33	26.0	5	
			1.67	> 26.0	(2)	Power Supply Limits
0	100	0	1.00	> 26.0	(2)	Buzz Starts at 22KV
			1.33	> 26.0	(2)	Buzz Starts at 24KV
			1.67	> 26.0	(2)	Buzzing
80	10	10	1.00	16.0	.2	
			1.33	17.0	1.0	
			1.67	18.5	12-22	
50	25	25	1.00	17.5	11-27	
			1.33	22.5	10-18	
			1.67	> 20.0	(1)	Buzzing
65	30	5	1.00	17.0	6-9	
			1.33	20.0	10-14	
			1.67	24.5	8	
65	10	25	1.0	17.5	1-2	
			1.33	20.0	10-20	
			1.67	21.0	12-15	

Notes: (1) Detector saturated immediately by surface spark. Could not obtain light pulse delay time.
(2) Power supply limited finding surface spark voltage level.

output signal as compared timewise with the peak current pulse. It can be seen that the light pulse delay time increases with an increase in gas pressure and mainly with an increase of CO_2 concentration. The results of these experiments helped in setting conditions for subsequent tests so that a corona discharge rather than a surface spark would be encountered.

Another important subject to be considered in this subsection is a comparison between preionization voltage and current in the laser and similar measurements in the corona discharge experiment. First, there is an 8.5:1 relation between the surface area of the corona dielectric plates in the laser and the 2.54 cm x 2.54 cm dielectric plate in the corona discharge experimental apparatus. Therefore, if we take the maximum and minimum values of "preionization current" found in Tables 10 and divide by 8.5, we see that the expected current in the corona discharge experiment should range from 45.2 amps to 21.7 amps. As we will see in the next subsection, this is the approximate range of current observed in the corona discharge experiment (see Table 5). This current level produces the corona glow condition described earlier. When surface sparking occurs, the current approaches 450 amps and the intensity of the optical pulse saturates the output of the photomultiplier tube. This occurs because the monochromator entrance and exit slits were adjusted to accept the weaker corona glow light levels. Figure 21 shows an oscilloscope photograph of anode voltage (V_A), current (I) and photomultiplier tube (PM) signals. The sudden collapse of anode voltage causes a large spike in current (450 amps) to occur which in turn produces a strong light signal which saturates the detector.

Figure 22 shows a typical response of a 2 mm thick MACOR\ plate subject to a 22.5 KV voltage pulse with a 30 n-sec rise time as recorded by a high speed storage oscilloscope. The gas was N_2 at 1 atm. Observable is a current pulse

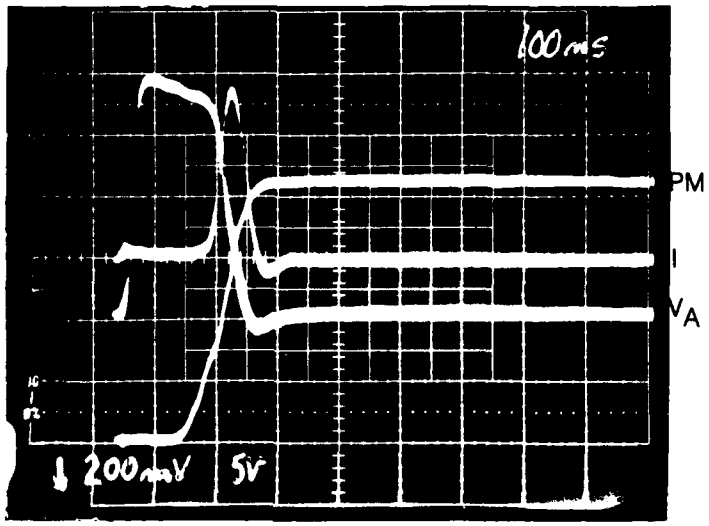

Figure 21. Oscilloscope traces of anode voltage (V_A), current (I) and photomultiplier tube outlet (PM) signals for conditions producing surface sparking in test no. 2.20.

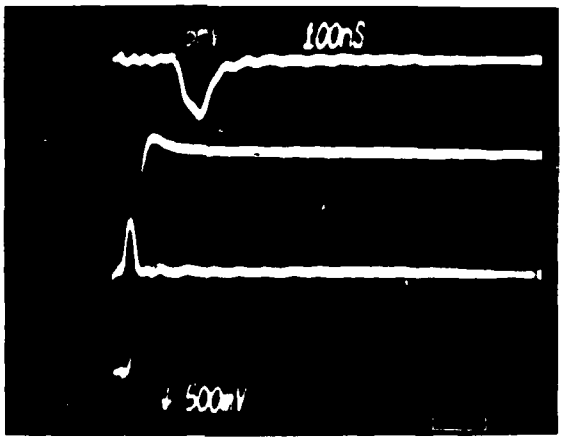

Figure 22. Corona discharge electrical (current and voltage) and optical signals at λ = 1750 Å.

having a peak value of 45 amps with a 20 n-sec half width. A single light pulse at 1750 A is indicated by the photomultiplier output signal. These signals are typical of what is observed for the weak or corona discharge regime.

The signals shown in Figure 22 are not exactly time correlated because a storage oscilloscope was used which accumulates these signals over 2 or 3 pulses. A dual beam oscilloscope was used to measure the time relationship between the traces, referenced to the peak in the voltage pulse. The current peak is actually shifted about 30 to 40 n-sec in time so that its peak is about 5 to 10 n-sec lagging the voltage peak. The light pulse peak lags the current pulse peak by 50-60 n-sec for this example. However, the displacement or lag in time varies with the gas composition used. Gas mixtures which are helium rich have longer delays between the applied voltage pulse and resultant light pulse.

The last subject to be treated in this subsection describes results of tests to measure the charge on the corona dielectric plate as a function of time. Figure 23 shows the test set-up in schematic form. Also shown is the probe design. Three measurement positions were probed as indicated in Fig. 23. The test gas was air at 1 atm. A 3 mm MACOR dielectric plate was used and the anode to cathode voltage was 21.5 KV.

Figure 24 shows the anode voltage and discharge current for the first 18μ-sec period. Note that the anode voltage starts at 21.5 KV and decreases to zero in small steps. At every step there is a small current spike (0.8 amps). Figure 25 shows anode voltage, probe voltage (for probe located at center of gap, 2 mm from the dielectric surface) and current for the first 450 n-sec. The voltage at the center is 14.0 KV. Measurements at 0.8 cm from the anode was 18.5 KV while at 0.8 cm from the cathode the voltage was 9.0 KV. Figure 26

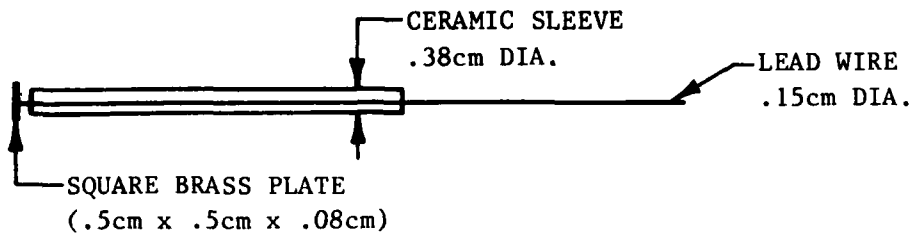

(a) Fine voltage probe design details.

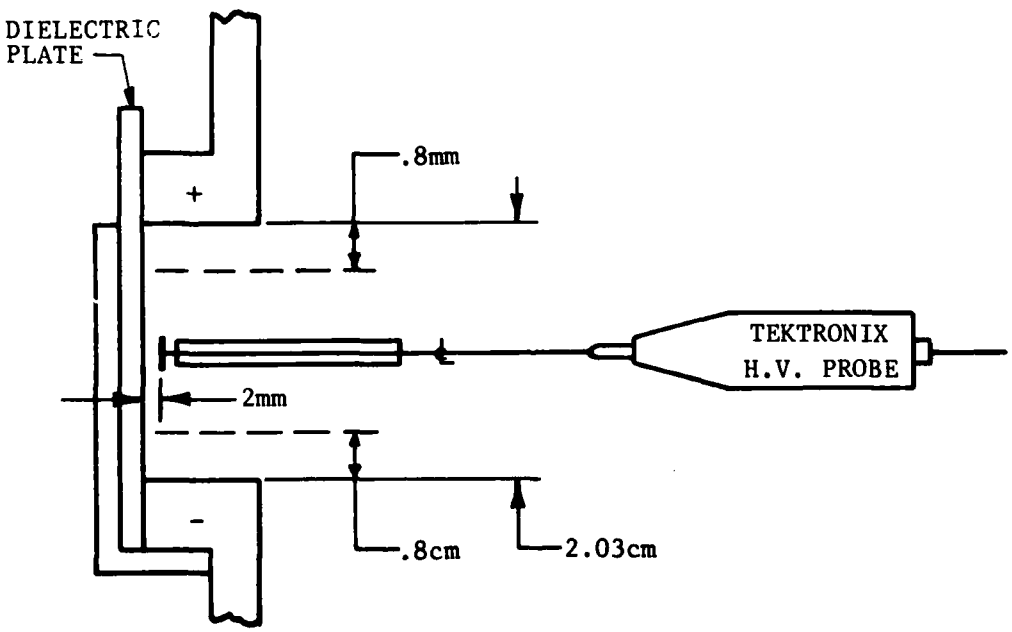

(b) Test setup for measuring charge on dielectric plate.

Figure 23. Schematic of experiment to measure charge decay on dielectric plate.

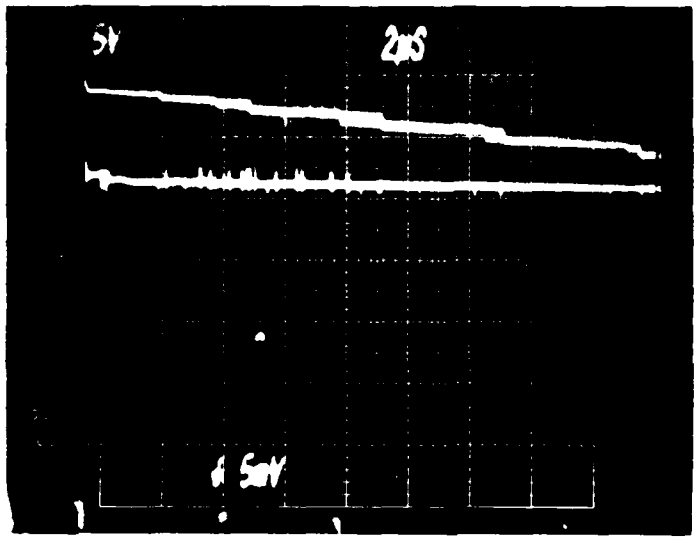

Figure 24. Anode voltage and discharge current. (Test no. 2.15)

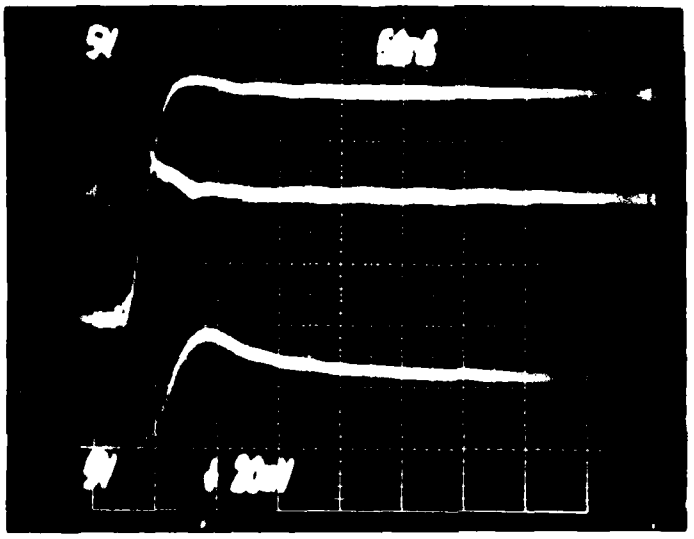

Figure 25. Variation of anode voltage, probe voltage (center location) and discharge current for first 450 n-seconds. (Test no. 2.15)

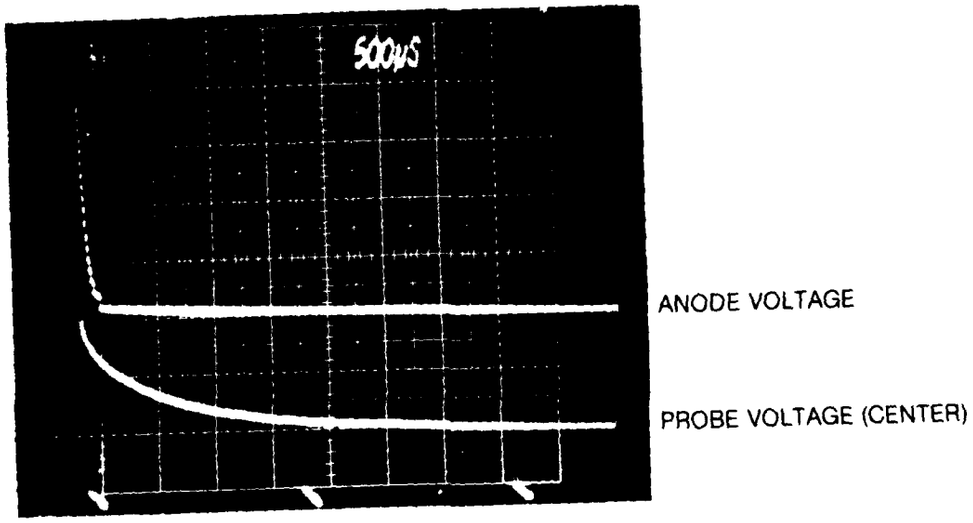

Figure 26. Decay of anode voltage and probe voltage (center location). (Test no. 2.15)

82-10-18-9

shows the decay of the anode voltage and probe voltage at the center of the gap. The anode voltage decays to zero in 170μ-sec whereas the dielectric voltage takes 6.5 m-sec to decay to zero. We have not made measurements of this nature in the laser as of this date. However, it is felt that strong ionic currents within the laser discharge gap may contribute to removing the charge on the dielectric in a shorter period of time than reported above.

Parametric Investigation of Corona Discharges

This portion of the experiment dealt with the measurement of electrical signals and spectral response of the ultraviolet light eminating from the corona discharge. Five series of tests are described which represent changes in physical parameters known to effect the corona discharge. These tests relate to changes in: gas composition, pressure level, dielectric thickness, anode to cathode gap length, and dielectric material. Table 4 summarizes the test variables involved and serves as an index. Also included in Table 4 are measured anode voltage and current as well as dV_A/dt, plasma current and dI/dt. The derivatives dV_A/dt and dI/dt were scaled from oscilloscope photographs and represent the steepest slopes. The plasma current is calcualted from equations (5) and (6) using measured capacitances from Table 5 for the various dielectric plates. Incidentally, equation (3) and values of the dielectric constant given in Table 2 adequately predicts the capacitance for the corona dielectric plate when the anode and cathode gap is 2.0 cm or greater. As the gap decreases, a non-linear relationship between surface area and capacitance develops that is not predictable by equation (3). The test set-up for this experiment was described in Section 4.0.

So that the resultant spectrums can be compared for the various test conditions, all tests were conducted in exactly the same manner. Table 6 summarizes the test procedures and measuring system parameters that were maintained.

Gas Composition Effects

Figure 27 shows the corona emission spectrum for the individual primary laser gases. The spectrum for CO_2 (top plot) shows little intensity over the 50% CO_2 and 50% He mixture. However, the spectrum obtained for nitrogen (lower plot) leaves no doubt that this gas dominates in the production of UV photons. This result is similar to the one for spark discharge preionization as reported by McKen, et al.[14].

Babcock[17] has shown that CO_2 absorbs strongly below 1150 Å. The absorption then decreases to a few cm^{-1} atm^{-1} in an 100 Å band centered around 1200 Å, then becomes strong again. The absorption again falls to about 2 cm^{-1} atm^{-1} at

TABLE 4. TEST SUMMARY FOR CORONA DISCHARGE EXPERIMENT

TEST NO.	DIELECTRIC THICK. (mm)	DIELECTRIC MAT'L.	ELECTRODE GAP (cm)	COMPOSITION			PRESS. (Atm)	ANODE VOLTAGE (kv)	$\frac{dV_a}{dt}$ (volts/sec)	DISCHARGE CURRENT (Amps)	PLASMA CURRENT (Amps)	$\frac{dI}{dt}$ (Amps/sec)
				H_e	CO_2	N_2						
2.01[1]	2.0	MACOR	2.03	0.0	0.0	100.0	1.14	22.0	9.00×10^{11}	52.4	-	-
2.02	2.0	MACOR	2.03	65.2	22.7	12.1	1.68	22.5	9.32×10^{11}	56.4	-	-
2.03	2.0	MACOR	2.03	65.2	22.7	12.1	1.68	22.5	-	56.0	-	-
2.04	2.0	MACOR	2.03	65.2	22.7	12.1	1.68	22.5	-	56.4	-	-
2.05	2.0	MACOR	2.03	65.2	22.7	12.1	1.68	22.5	-	56.4	-	-
2.06	2.0	MACOR	2.03	65.2	22.7	12.1	1.68	22.5	9.38×10^{11}	52.4	49.21	3.74×10^{9}
2.07	2.0	MACOR	2.03	0.0	0.0	100.0	1.5	22.0	8.35×10^{11}	52.4	49.56	4.53×10^{9}
2.08	2.0	MACOR	2.03	0.0	100.0	0.0	1.5	22.0	8.33×10^{11}	52.4	49.57	4.03×10^{9}
2.09[1]	2.0	MACOR	2.03	100.0	0.0	0.0	1.5 2.0	17.5	6.70×10^{11}	450.0	447.72	10.29×10^{9}
2.10	2.0	MACOR	2.03	50.0	50.0	0.0	1.5	17.5	6.70×10^{11}	32.2	29.92	2.23×10^{9}
2.11[1]	2.0	MACOR	2.03	80.0	10.0	10.0	1.5	17.5	8.33×10^{11}	35.5	32.67	2.69×10^{9}
2.12	2.0	MACOR	2.03	65.0	30.0	5.0	1.5	22.5	8.20×10^{11}	56.4	53.61	4.18×10^{9}
2.13[1]	2.0	MACOR	2.03	65.5	14.5	20.0	1.5	22.5	8.33×10^{11}	58.0	55.17	4.03×10^{9}
2.14	2.0	MACOR	2.03	65.0	19.2	15.8	1.5	22.5	8.33×10^{11}	53.2	50.37	4.03×10^{9}

NOTES:
1. POSSIBLE SURFACE SPARK
2. FINE VOLTAGE PROBE USED FOR V(t)
3. SCOPE PHOTOS - DUAL BEAM VS STORAGE
4. 451 AMPS WHEN VOLTAGE COLLAPSES

TABLE 4. TEST SUMMARY FOR CORONA DISCHARGE EXPERIMENT

TEST NO.	DIELECTRIC THICK. (mm)	DIELECTRIC MAT'L.	ELECTRODE GAP (cm)	COMPOSITION			PRESS. (Atm)	ANODE VOLTAGE (kv)	$\frac{dV_a}{dt}$ (volts/sec)	DISCHARGE CURRENT (Amps)	PLASMA CURRENT (Amps)	$\frac{dI}{dt}$ (Amps/sec)
				H_e	CO_2	N_2						
2.15[2]	3.0	MACOR	2.03	-	AIR	-	1.0	21.5	6.67×10^{11}	23.4	21.53	9.85×10^{8}
2.16[3]	3.0	MACOR	2.03	-	AIR	-	1.0	19.0	8.33×10^{11}	23.7	21.37	1.76×10^{9}
2.17	3.0	MACOR	2.03	0.0	0.0	100.0	1.5	18.0	8.33×10^{11}	18.5	16.17	1.23×10^{9}
2.18	3.0	MACOR	2.03	0.0	0.0	100.0	1.0	19.0	8.33×10^{11}	17.8	15.47	1.24×10^{9}
2.19	3.0	MACOR	2.03	0.0	0.0	100.0	0.5	14.5	5.00×10^{11}	13.7	12.3	1.12×10^{9}
2.20[6]	3.0	MACOR	2.03	0.0	0.0	100.0	0.5	19.0	6.75×10^{11}	451.0 29.0	449.11	4.57×10^{10}
2.21	3.0	MACOR	2.03	0.0	0.0	100.0	2.0	19.0	6.25×10^{11}	20.1	18.35	2.05×10^{9}
2.22	3.0	MACOR	2.03	65.5	22.8	12.2	1.0	17.0	6.25×10^{11}	16.7	14.95	4.89×10^{8}
2.23	3.0	MACOR	2.03	65.0	22.8	12.2	1.0	17.0	6.25×10^{11}	16.6	14.85	1.68×10^{9}
2.24	1.0	MACOR	2.03	65.0	22.8	12.2	1.0	17.0	6.56×10^{11}	20.1	15.57	1.21×10^{9}
	1.0	MACOR	2.03	65.0	22.8	12.2	1.5	17.0	6.25×10^{11}	15.3	11.11	9.46×10^{8}
2.26	1.0	MACOR	2.03	65.0	22.8	12.2	1.5	20.0	8.33×10^{11}	19.3	13.55	1.29×10^{9}
2.27	1.0	MACOR	2.03	65.0	22.8	12.2	1.5	14.0	5.76×10^{11}	10.1	6.13	6.5×10^{8}
2.28	1.0	MACOR	2.03	65.0	22.8	12.2	2.0	17.0	6.25×10^{11}	13.7	9.39	8.06×10^{8}

TABLE 4. TEST SUMMARY FOR CORONA DISCHARGE EXPERIMENT

TEST NO.	DIELECTRIC THICK. (mm)	DIELECTRIC MAT'L.	ELECTRODE GAP (cm)	COMPOSITION			PRESS. (Atm)	ANODE VOLTAGE (kv)	$\frac{dV_a}{dt}$ (volts/sec)	DISCHARGE CURRENT (Amps)	PLASMA CURRENT (Amps)	$\frac{dI}{dt}$ (Amps/sec)
				H_e	CO_2	N_2						
2.29	1.0	MACOR	2.03	0.0	0.0	100.0	1.0	19.0	7.14×10^{11}	19.3	16.90	1.37×10^{9}
2.30	2.0	MACOR	2.03	65.0	22.8	12.2	1.0	17.0	6.25×10^{11}	19.33	15.02	9.28×10^{8}
2.31	2.0	MACOR	2.03	65.0	22.8	12.2	1.5	17.0	6.25×10^{11}	11.68	9.55	7.45×10^{8}
2.32	2.0	MACOR	2.03	65.0	22.8	12.2	2.0	17.0	6.56×10^{11}	11.3	9.07	6.84×10^{8}
2.33	2.0	MACOR	2.03	0.0	0.0	100.0	1.0	19.0	8.33×10^{11}	18.5	15.50	1.34×10^{9}
2.34	2.0	MACOR	1.27	65.0	22.8	12.2	1.0	9.5	3.33×10^{11}	6.04	3.94	2.19×10^{8}
2.35	2.0	MACOR	1.27	65.0	22.8	12.2	1.0	10.0	3.57×10^{11}	6.44	4.19	3.89×10^{8}
2.36	2.0	MACOR	1.27	65.0	22.8	12.2	1.0	9.5	3.40×10^{11}	6.24	4.10	2.34×10^{8}
2.37	2.0	MACOR	1.65	65.0	22.8	12.2	1.0	10.0	3.00×10^{11}	6.04	4.51	2.24×10^{8}
2.38	2.0	MACOR	2.03	65.0	22.8	12.2	1.0	10.0	3.75×10^{11}	5.44	4.17	2.22×10^{8}
2.39	2.0	ZERODUR	2.03	65.0	22.8	12.2	1.0	15.0	4.60×10^{11}	14.50	12.30	9.67×10^{8}
2.40	2.0	ZERODUR	2.03	65.0	22.8	12.2	1.0	16.0	5.00×10^{11}	16.11	13.91	3.02×10^{8}
2.41	2.0	ZERODUR	2.03	65.0	22.8	12.2	1.0	10.0	2.33×10^{11}	6.85	5.82	3.22×10^{8}

TABLE 5. MEASURED CAPACITANCE FOR THE CORONA DIELECTRIC PLATES USED IN EXPERIMENT

DIELECTRIC MATERIAL	THICKNESS (mm)	GAP (cm)	CAPACITANCE (pF)
MACOR	2.0	2.03	3.4
MACOR	2.0	1.65	5.1
MACOR	2.0	1.27	6.3
MACOR	1.0	2.03	6.9
MACOR	3.0	2.03	2.8
ZERODUR	2.0	2.03	4.4

TABLE 6. TEST PROCEDURES AND MEASUREMENT PARAMETERS COMMON TO ALL CORONA DISCHARGE TESTS

Monochromator:	Slits: 250 μm, Window Material: LiF Wavelength Scan: 1050 Å to 2000 Å Autoscan: 50Å/min.
Photomultiplier:	Type: EMI Model 9635 B Volts O/A Sensitivity: 5000 Amps/Lumen @ 940 Volts O/A Dark Current: 2.0 n-amps.
Strip Chart Recorder:	Scale: 0.5 V/in, Speed: 100 sec/in.
Pulser:	Pulse Repetition Frequency: 2 pps.

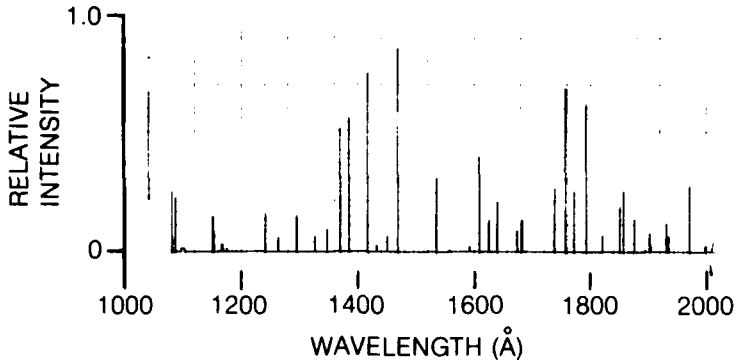

(a) CO_2 (TEST NO. 2.08)

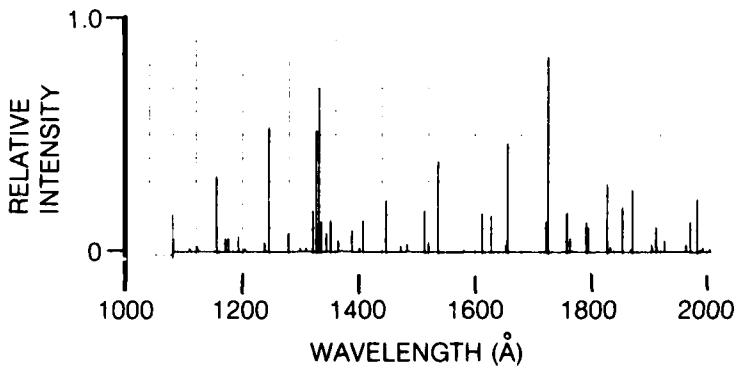

(b) 50% CO_2, 50% He (TEST NO. 2.10)

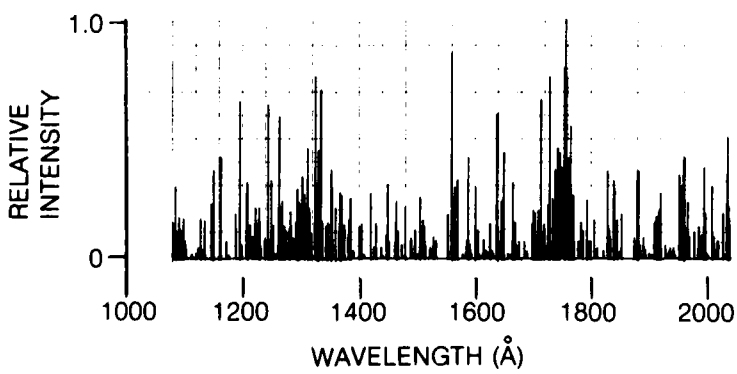

(c) N_2 (TEST NO. 2.07)

Figure 27. Corona emission spectrum for individual primary laser gases.

82-10-18-10

1600 Å and continues to decrease thereafter, reaching a negligible level at about 1950 Å. Therefore, Babcock concludes that the only UV photons which could penetrate CO_2 sufficiently were the two groups 1170 Å < λ <1240 Å and λ>1600 Å.

Figure 28 shows the corona emission spectrum for two typical laser gas mixtures; a 23% CO_2, 12% N_2, 65%, He mixture and a 10% CO_2, 10% N_2, and 80% He mixture. This figure corroborates Babcock's findings in that mixture with 23% CO_2 has very little UV activity below 1550 Å whereas the 10% CO_2 mixture has significant UV emission intensity in the 1150-1300 Å region. It should be pointed out that the very short path length in this experiment is quite different than that in Babcock's experiments. Figure 27 does show that UV radiation in the λ> 1600 Å range predominates in the production of UV photons.

Pressure Level Effects

Tests 2.24, 2.25 and 2.28 having pressures of 1.0, 1.5 and 2.0 atm respectively have been isolated for this study. Figure 29 compares the light emission spectrum for these tests for a 65% He, 22.8% CO_2 and 12.2% N_2 gas mixture. The anode voltage was kept constant at 17.0 KV. A 1.0 mm thick MACOR dielectric plate was used having an anode to cathode gap of 2.03 cm. A comparison of Figs. 29, (b) and (c) shows that in general the UV light output decreases as pressure increases. The continuum radiation evident at 1.0 atm is significantly reduced at 1.5 atm and is nearly zero at 2.0 atm. An examination of Table 4 shows that for a rather small change in dV_A/dt, the plasma current (I_p) and dI/dt decrease significantly as the pressure is increased. As will become evident from this and other comparisons which follow, the time rate of change of current (I) with time is primarily responsible for the light output. This parameter is related to the energy deposited into the plasma as discussed in Section 3. The greater dI/dt the more intense is the UV light signal.

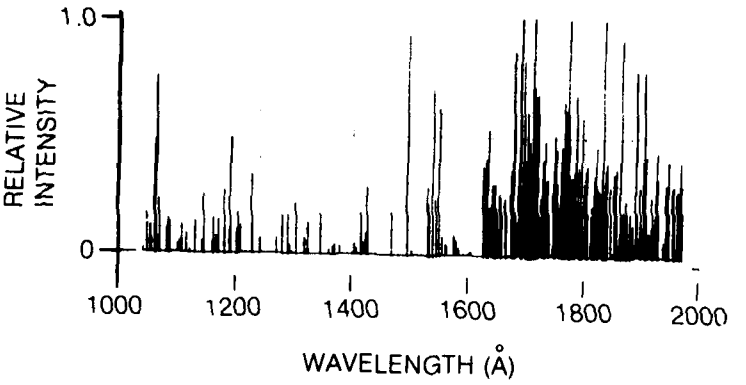

(a) 23% CO_2, 12% N_2, 65% He (TEST NO. 2.06)

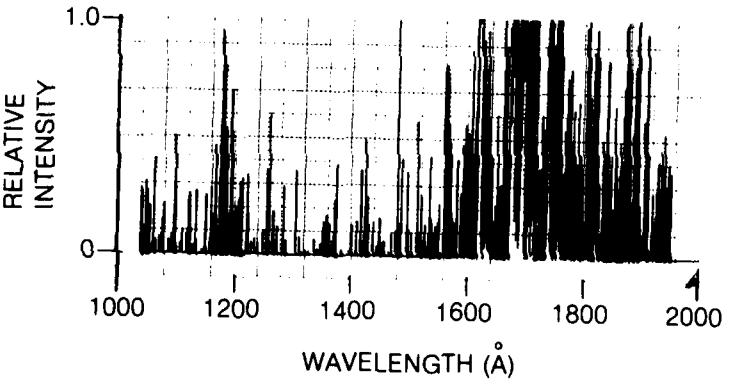

(b) 10% CO_2, 10% N_2, 80% He (TEST NO. 2.11)

Figure 28. Corona emission spectrum for two typical laser gas mixtures.

82-10-18-11

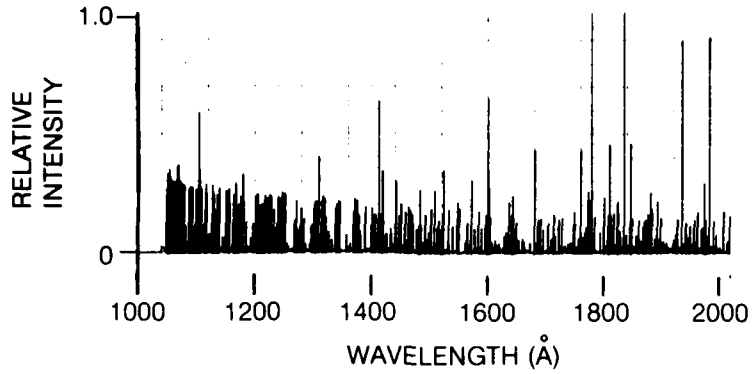

(a) GAS PRESSURE = 1.0 atm (TEST NO. 2.24)

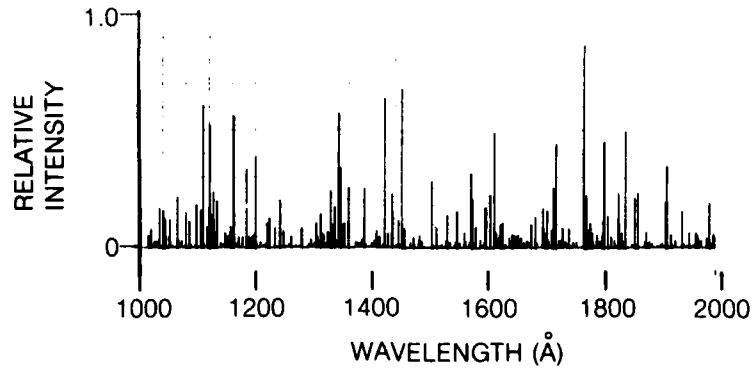

(b) GAS PRESSURE = 1.5 atm (TEST NO. 2.25)

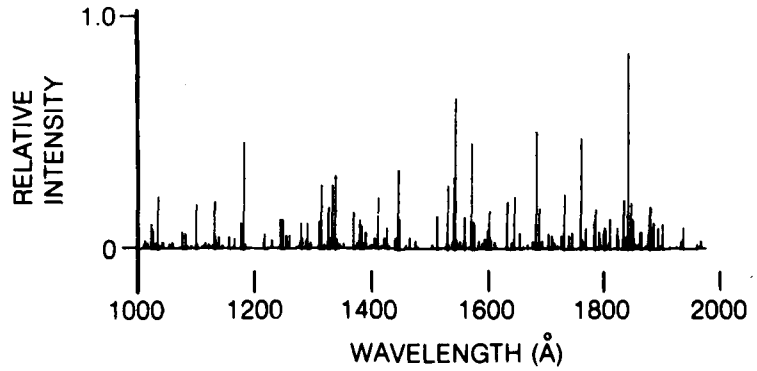

(c) GAS PRESSURE = 2.0 atm (TEST NO. 2.28)

Figure 29. Comparison of light emission spectrum for three pressure levels of a $He/CO_2/N_2$: 65.0/22.8/12.2 gas pressure. Anode voltage is 17.0 KV. A 1.0 mm MACOR dielectric plate was used.

82-10-18-12

An examination of results from tests 2.30, 2.31 and 2.32 for the same conditions except use of a 2.0 mm dielectric plate gave the same qualitative results as discussed above.

Dielectric Thickness Effects

For this important test series, 2 sets of test data have been selected to study the effects of changing dielectric thickness while maintaining all other parameters constant. These test results will help explain observations made in the laser output measurement experiment. Tests 2.22, 2.30 and 2.24 present data for a MACOR plate thicknesses of 3.0, 2.0 and 1.0 mm respectively. At 1.0 atm, 65% He, 2.28% CO_2 and 12.2 N_2 laser gas mixture was used. The anode voltage was 17.0 KV. Figure 30 distinctly shows that the UV light signal strength increases as the plate thickness decreases. In fact, for the 1.0 mm plate thickness, there is more activity over the entire spectrum as compared to the 2.0 and 3.0 mm thickness spectrums. However, the difference between the 2.0 and 3.0 mm thicknesses is not as great as that between the 1.0 and 2.0 mm thickness.

Figure 31 presents spectral data for a 3.0, 2.0 and 1.0 mm thick MACOR plate for a 1.0 atm, N_2 gas. The corresponding anode voltage was 19.0 KV. The same trend is observed but not as clearly as for the laser gas mixture.

The reason for the increase in UV light intensity as the thicknes of the dielectric plate is reduced is due to the higher rate of energy deposition into the plasma. This is evident by an increase in plasma current and dI/dt as shown in Tables 7 and 8 which have been extracted from Table 4. For an approximately constant dV_A/dt, the current pulse responds faster due to a decreased system capacitance as thickness is decreased. A comparison between Tables 7 and 8 also indicates that dI/dt changes less for the N_2 case than

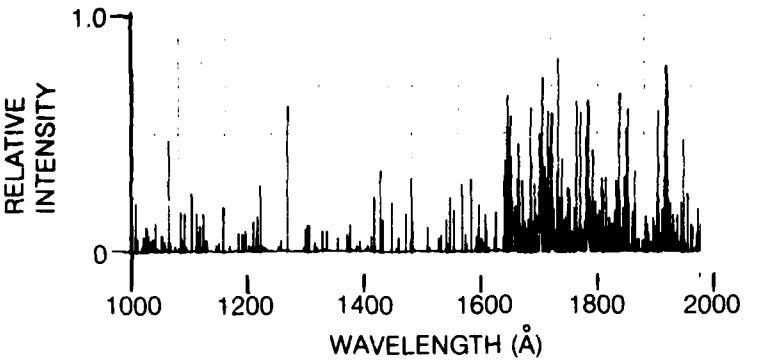

(a) MACOR THICKNESS = 3.0 mm (TEST NO. 2.22, 2.23)

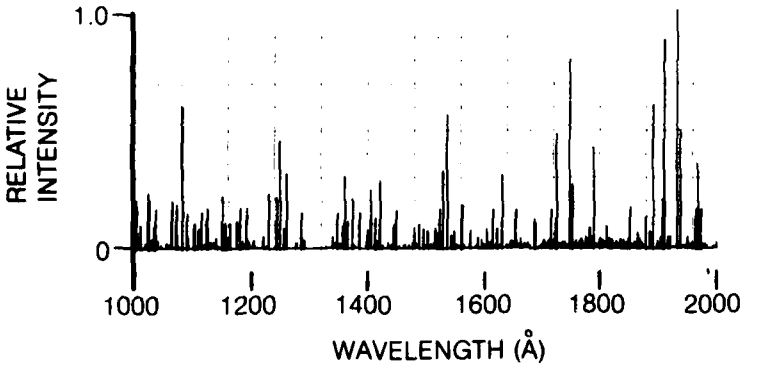

(b) MACOR THICKNESS = 2.0 mm (TEST NO. 2.30)

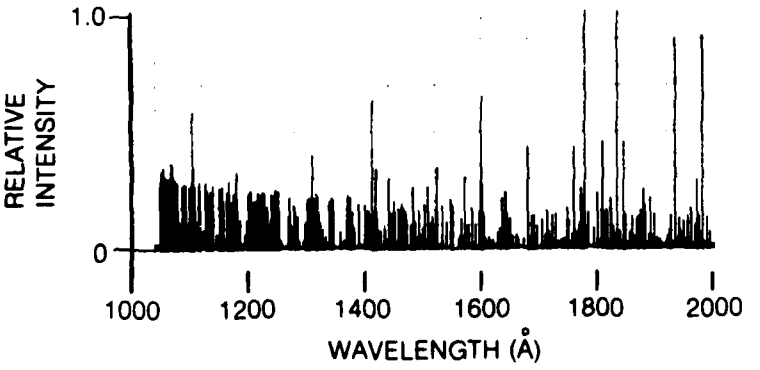

(c) MACOR THICKNESS = 1.0 mm (TEST NO. 2.24)

Figure 30. Comparison of light emission spectrum for three thicknesses of corona dielectric for a $He/CO_2/N_2$: 65.0/22.8/12.2 gas mixture at 1 atm and an anode voltage of 17.0 KV.

82-10-18-13

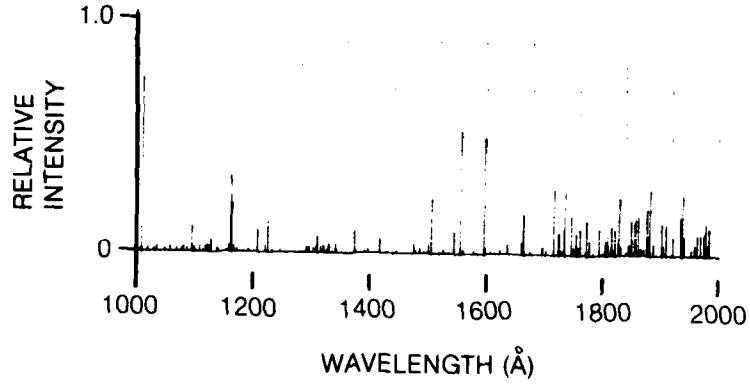

(a) MACOR THICKNESS = 3.0 mm (TEST NO. 2.18)

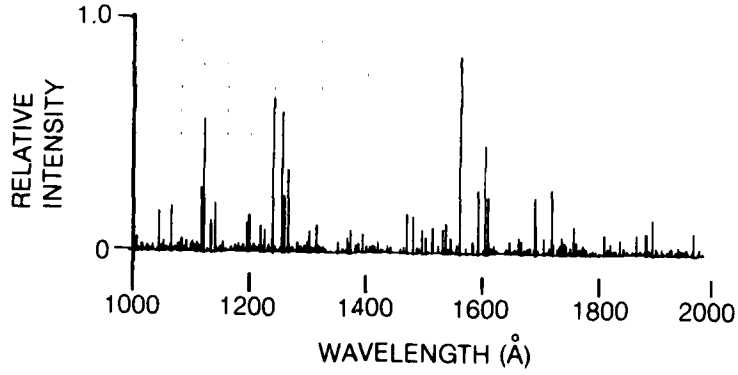

(b) MACOR THICKNESS = 2.0 mm (TEST NO. 2.33)

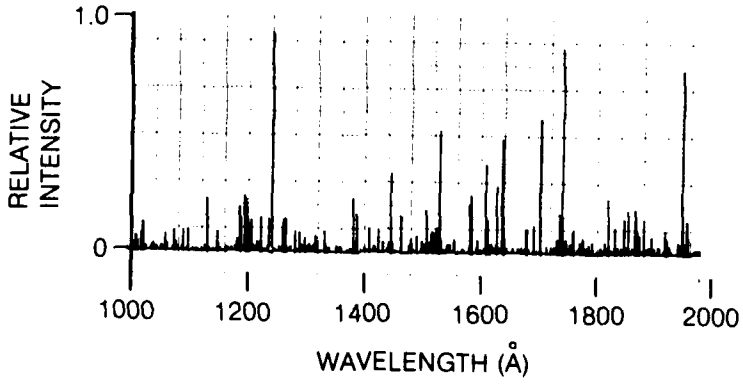

(c) MACOR THICKNESS = 1.0 mm (TEST NO. 2.29)

Figure 31. Comparison of light emission spectrum for three thicknesses of corona dielectric for pure N_2 gas at 1 atm and as anode voltage of 19.0 KV.

82-10-18-14

TABLE 7. SUMMARY OF ELECTRICAL PARAMETERS FROM THICKNESS COMPARISON TESTS FOR A TYPICAL 1.0 ATM LASER GAS MIXTURE (65% He, 22.8% CO_2, 12.2% N_2). ANODE VOLTAGE IS 17.0 KV

TEST NO.	MACOR THICK (mm)	CURRENT I Amps	$\frac{dV_A}{dt}$ (Volts/sec)	CAPACITANCE (pF)	DISPL. CURRENT I_D (Amps)	PLASMA CURRENT I_p (Amps)	$\frac{dI}{dt}$ (Amp/sec)
2.22	3.0	16.70	6.25×10^{11}	2.8	1.75	14.95	4.89×10^{8}
2.30	2.0	19.30	6.25×10^{11}	3.4	4.31	15.02	9.28×10^{8}
2.24	1.0	20.10	6.56×10^{11}	6.9	4.53	15.57	1.21×10^{9}

TABLE 8. SUMMARY OF ELECTRICAL PARAMETERS FROM THICKNESS COMPARISON TESTS FOR A TYPICAL 1.0 ATM PURE N_2 GAS. ANODE VOLTAGE IS 19.0 KV.

TEST NO.	MACOR THICK (mm)	CURRENT I Amps	$\frac{dV_A}{dt}$ (Volts/sec)	CAPACITANCE (pF)	DISPL. CURRENT I_D (Amps)	PLASMA CURRENT I_p (Amps)	$\frac{dI}{dt}$ (Amp/sec)
2.18	3.0	17.80	8.33×10^{11}	2.8	2.33	15.47	1.24×10^{9}
2.33	2.0	18.50	8.33×10^{11}	3.4	2.83	15.50	1.34×10^{9}
2.29	1.0	19.30	7.14×10^{11}	6.9	2.40	16.90	1.37×10^{9}

for the laser gas case as observed from the spectral data. For the laser gas (Table 6), dI/dt changes from 4.89×10^8 to 1.21×10^9 amps/sec as compared to the corresponding values (Table 8) for N_2, 1.24×10^9 to 1.37×10^9.

Anode To Cathode Gap

Figure 32 compares the UV light emission spectrum for three anode to cathode gap lengths for a 2.0 mm thick MACOR dielectric plate. A 1.0 atm laser gas mixture (65% He, 2.28% CO_2, 12.2% N_2) was used during these tests. The anode voltage was maintained constant at 10.0 KV. It was necessary to operate at 10.0 KV to prevent surface sparking at 1.27 cm. This voltage level was then kept constant for the other gaps. Test 2.38 had an electrode gap of 2.03 cm, Test 2.37 a gap of 1.65 cm and Test 2.35 a gap of 1.27 cm. A comparison of Figures 32 (a), (b) and (c) shows the obvious result, namely, that as the gap is decreased, the light intensity increases. For the 1.27 cm electrode gap, Fig. 5-17 (c) shows very intense activity over the entire spectrum from 1050 to 2000 Å. The detector was saturated most of the time above 1700 Å. During this test, the anode voltage and gap current were monitored on an oscilloscope and surface sparking did not occur. The increase in light intensity between 2.03 cm and 1.65 cm is not as great as between 1.65 and 1.27 cm. Table 4 again indicates that dI/dt increases as the gap length between anode and cathode decreases.

Dielectric Material Effect

Figure 33 shows a comparison of the UV light emission spectra for 2 dielectric plate materials. Figure 33 (a) shows the results for ZERODUR, a ceramic having extremely low thermal expansion. Figure 33 (b) show similar results for MACOR. The material properties for these ceramics are given in Table 2. For comparable test conditions, ZERODUR produced a more intense light output than MACOR. As before, the reason is that dI/dt is greater for

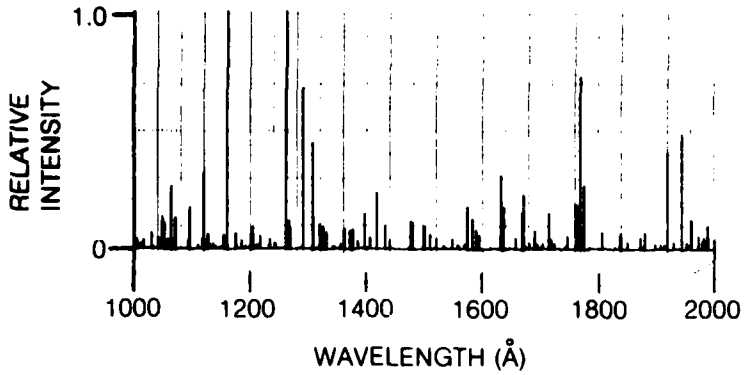

(a) ELECTRODE GAP = 2.03 cm (TEST NO. 2.38)

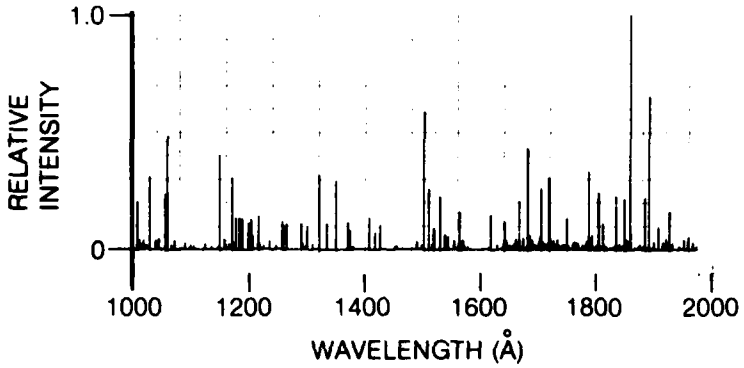

(b) ELECTRODE GAP = 1.65 cm (TEST NO. 2.37)

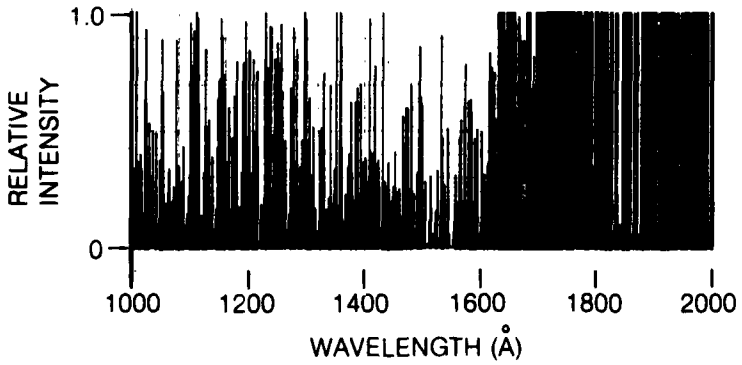

(c) ELECTRODE GAP = 1.27 cm (TEST NO. 2.35)

Figure 32. Comparison of light emission spectrum for three electrode gaps for a 2.0 mm thick MACOR dielectric plate. Gas mixture is $He/CO_2/N_2$: 65.0/22.8/12.2 at 1 atm and anode voltage of 10.0 KV.

82-10-18-15

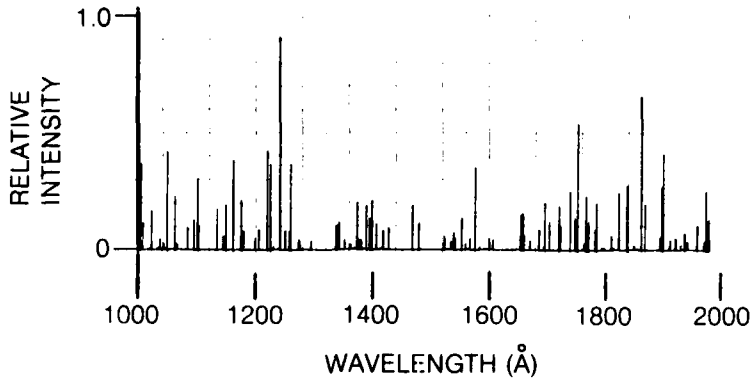

(a) ZERODUR PLATE (TEST NO. 2.41)

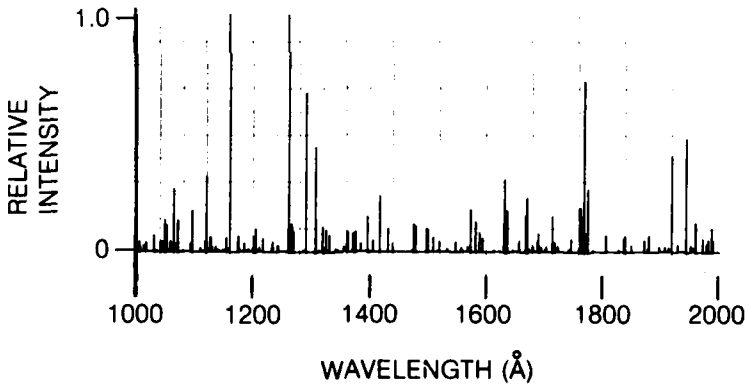

(b) MACOR PLATE (TEST NO. 2.38)

Figure 33. Comparison of light emission spectrum for 2 different corona dielectric materials, 2 mm thick. Gas mixture is $He/CO_2/N_2$: 65.0/22.8/12.2 at 1.0 atm and anode voltage of 10.0 KV.

82-10-18-16

ZERODUR than for MACOR. It should be noted that ZERODUR produces more activity in the 1050 to 1300 Å and 1800 to 2000 Å spectral regions than does MACOR.

Laser Preionization Measurement Experiment

As discussed in Section 4.0, the purpose of this experiment was to simultaneously measure the UV light output from the corona dielectric and the resultant preionization electron density. The laser shown in Fig. 11 was inserted in one of the arms of the microwave interferometer shown schematically in Fig. 13. However, because the vacuum UV monochromator was being used concurrently in the corona discharge experiment, the laser was not attached to it as shown in Fig. 12. Eight tests were performed using the X-band (10.2 G-Hz frequency) microwave system. The tests spanned a range of typical laser gas mixtures, voltages, and pressures. During testing, it was found that preionization electron density could not be measured because of a large noise spike accompaning the voltage switching transient. This noise lasted approximately 40-60 n-sec from the start of the voltage pulse and completely eliminated the measurement of the desired preionization pulse. Considerable effort was expended to mimimize the amplitude of the noise signal but to no avail. Measurement of the main discharge electron density (peak values) were possible and were determined to be between 1.0×10^{11} and 4.0×10^{11} electrons/cc. However, using measured oscilloscope traces of electrode gap voltage and current (similar to Fig. 34) and elecron drift

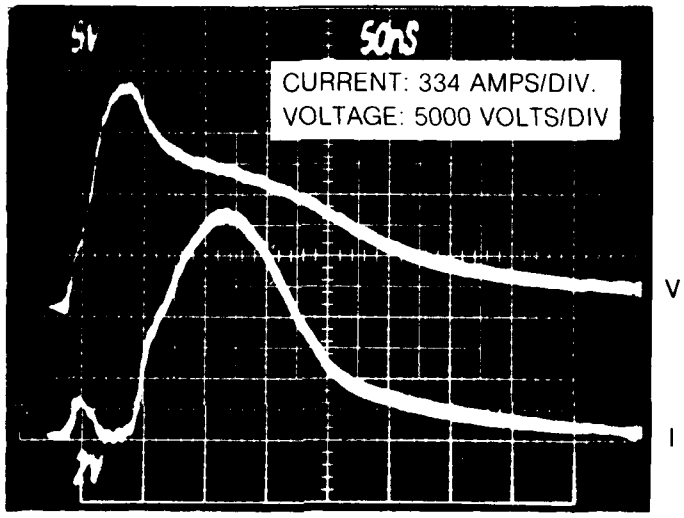

Figure 34. Current and voltage waveforms from CO_2 TEA laser discharge.

82-10-18-17

velocity from measured atomic cross-section data gave electron densities of approximately 5 X 10^{13} to 1.1 X 10^{14} electrons/cc using equation (7).

$$n_e = J/(e\ V_D) \qquad (7)$$

where e is the charge on an electron and V_D is the electron drift velocity. Figure 35 shows a plot of electron density versus time for a 1 atm laser gas mixture (10% CO_2, 10% N_2, 80% He). The difference in electron density as inferred from the two techniques results from the fact that plasma cutoff is well below the actual electron density in the laser. Cutoff for 10.2 G-Hz is 1.29 X 10^{12} electrons/cc. Therefore, it has been experimentally determined that the X-band microwave frequency is inappropriate for measuring main discharge electron density. To circumvent these problems, arrangements were made to install a 70 G-Hz microwave system employing signal processing in an attempt to measure electron density of both the preionization and main discharges. However, due to contract termination, the 70 G-Hz system was never used.

Laser Output Measurement Experiment

A series of 30 tests were performed to determine the effect of changes of corona dielectric thickness on laser output and electrical characteristics with all other parameters held fixed. Table 9 summarizes all of the important test parameters. The laser was not attached to the monochromator for these tests. For these tests, MACOR^R was the dielectric material having thickness of 1.0, 2.0, and 3.0 mm. The distance between anode and cathode was 2.0 cm. The anode voltage was held constant at 18.5 KV, with a storage capacitor of 10.0 nF and pulse repetition rate of 1 pps. The gas consisted of a 1 atm mixture of 65% He with varying amounts of N_2 and CO_2 (N_2/ (N_2 + CO_2) = 0.187 to 0.85). The gas discharge volume was 10.7 cc's. A stable resonator having a flat reflector, an 82% ZnSe partial reflector and apertured to 8.5 mm was utilized.

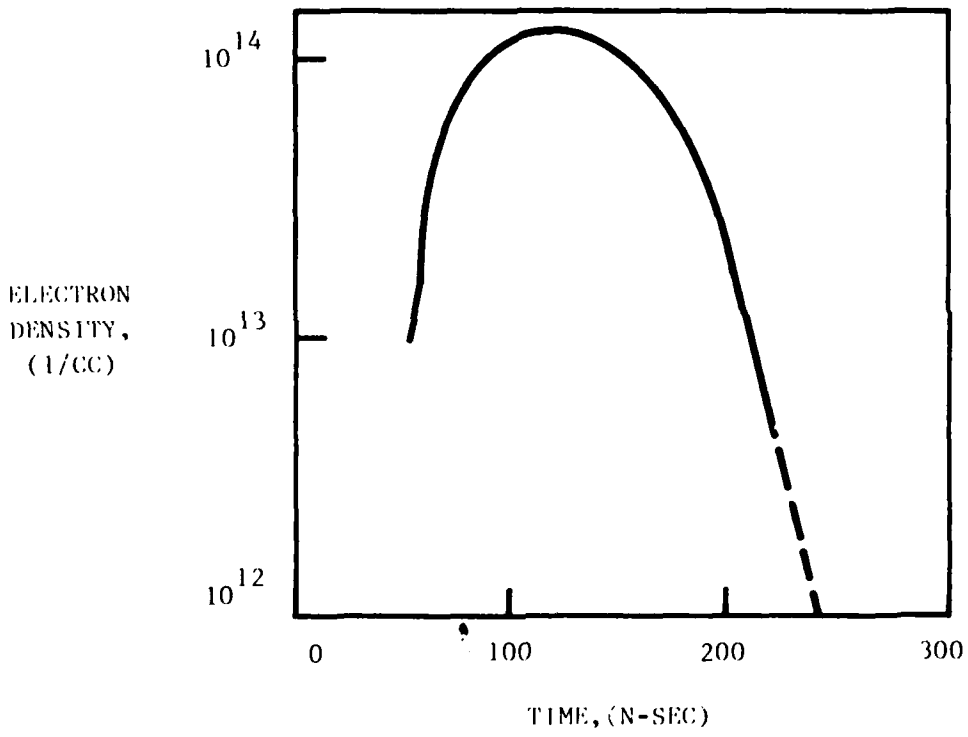

Figure 35. Electron density derived from V(t), I(t) and electron drift velocity. A 1.0 Atm mixture of 10% CO_2, 10% N_2 and 8% He was used.

TABLE 9. CO_2 TEA LASER TEST DATA SHEETS

CO_2 TEA LASER TEST SUMMARY (FLOWING TESTS)

LASER BUILD: #4A(Plexiglass)
OUTPUT MIRROR: 82%
REFLECTOR: FLAT (ES)
APERTURES: 2-8.5 mm
LOAD RES.: 3.33 kΩ
CHARGE RES.: 10MΩ
STORAGE CAP.: 10 nF

POWER SUPPLY: ADV. HIGH VOLT.
PHOTON DRAG DET: EL-OP(#1)
ENERGY METER: SCIENTEK(#1)
LASER PRESS: 1.0 ATM
PULSE REP RATE: 1.0 PPS
TOTAL LASER FLOW: 5.85 l/min

DATE: 12/7/82
NAME: WRK.

CORONA DIELECTRIC MTL.: MACOR
DIELECTRIC THICKNESS: 1.0 mm

TEST NO.	$\%H_e$	$\frac{N_2}{N_2+CO_2}$	CO_2 FLOW (l/min)	H_R FLOW (l/min)	N_2 FLOW (l/min)	ANODE VOLTAGE (KV)	PEAK CURRENT (AMPS)	PREION. CURRENT (AMPS)	OPTICAL PULSE ENERGY (JOULES)	PEAK OPTICAL POWER (KW)	COMMENTS
4.12	65	.350	1.32	3.28	0.72	18.5	1252	167	.048	462	
4.13	65	.286	1.46	3.28	0.59	18.5	1219	217	.042	378	
4.14	65	.143	1.76	3.28	0.29	18.5	1253	200	.026	451	
4.15	65	.571	0.88	3.28	1.17	18.5	1252	251	.039	262	
4.16	65	.714	0.59	3.28	1.46	19.0	1486	317	.002	0	ARCING
4.17	65	.857	0.29	3.28	1.76	18.5	--	-	0	0	ARCING
4.18	65	.450	1.13	3.28	0.92	18.5	1770	267	.052	409	
4.19	65	.143	1.76	3.28	0.29	18.5	1253	200	.026	367	REPEAT 4.12
4.20	65	.200	1.64	3.28	0.41	19.0	1353	184	.036	378	
4.21	65	.143	1.76	3.28	0.29	18.5	1253	200	.023	315	REPEAT 4.12

TABLE 9. CO_2 TEA LASER TEST DATA SHEETS

CO_2 TEA LASER TEST SUMMARY (FLOWING TESTS)

LASER BUILD: #4A(Plexiglass)
OUTPUT MIRROR: 82%
REFLECTOR: FLAT (ES)
APERTURES: 2-8.5 mm
LOAD RES.: 3.33 kΩ
CHARGE RES.: 10MΩ
STORAGE CAP.: 10 nF

POWER SUPPLY: ADV. HIGH VOLT.
PHOTON DRAG DET: EL-OP(#1)
ENERGY METER: SCIENTEK(#1)
LASER PRESS: 1.0 ATM
PULSE REP RATE: 1.0 PPS
TOTAL LASER FLOW: 5.85 1/min

DATE: 12/3/82
NAME: WRK.

CORONA DIELECTRIC MTL.: MACOR
DIELECTRIC THICKNESS: 2.0 mm

TEST NO.	$\%H_e$	$\frac{N_2}{N_2+CO_2}$	CO_2 FLOW (l/min)	H_R FLOW (l/min)	N_2 FLOW (l/min)	ANODE VOLTAGE (KV)	PEAK CURRENT (AMPS)	PREION. CURRENT (AMPS)	OPTICAL PULSE ENERGY (JOULES)	PEAK OPTICAL POWER (KW)	COMMENTS
4.01	65	.350	1.32	3.28	0.72	20	1670	234	.037	336	
4.02	65	.857	0.29	3.28	1.76	20	1436	217	.001	0	OCCASIONAL ARCING
4.03	65	.714	0.59	3.28	1.46	20	1470	234	.021	136	
4.04	65	.571	0.88	3.28	1.17	20	1837	267	.045	199	
4.05	65	.143	1.76	3.28	0.29	20	1670	184	.018	204	
4.06	65	.286	1.46	3.28	0.59	20	1570	200	.032	283	
4.07	65	.350	1.32	3.28	0.72	20	1703	233	.049	357	
4.08	50	.500	1.46	2.93	1.46	20	902	184	0	0	ARCING
4.09	70	.500	0.88	4.10	0.88	20	1737	234	0	0	ARCING
4.10	80	.500	0.59	4.68	0.59	20	2088	267	0	0	ARCING
4.11	65	.450	1.13	3.28	0.92	20	1870	284	.052	289	

TABLE 9. CO_2 TEA LASER TEST DATA SHEETS

CO_2 TEA LASER TEST SUMMARY (FLOWING TESTS)

LASER BUILD: #4A(Plexiglass)
OUTPUT MIRROR: 82%
REFLECTOR: FLAT (ES)
APERTURES: 2-8.5 mm
LOAD RES.: 3.33 kΩ
CHARGE RES.: 10MΩ
STORAGE CAP.: 10nF

POWER SUPPLY: ADV. HIGH VOLT.
PHOTON DRAG DET: EL-OP(#1)
ENERGY METER: SCIENTEK(#1)
LASER PRESS: 1.0 ATM
PULSE REP RATE: 1.0 PPS
TOTAL LASER FLOW: 5.85 l/min

DATE: 12/7/82
NAME: WRK.

CORONA DIELECTRIC MTL.: MACOR
DIELECTRIC THICKNESS: 3.0 mm

TEST NO.	$\%H_e$	$\frac{N_2}{N_2+CO_2}$	CO_2 FLOW (l/min)	H_R FLOW (l/min)	N_2 FLOW (l/min)	ANODE VOLTAGE (KV)	PEAK CURRENT (AMPS)	PREION. CURRENT (AMPS)	OPTICAL PULSE ENERGY (JOULES)	PEAK OPTICAL POWER (KW)	COMMENTS
4.22	65	.350	1.32	3.28	0.72	18.5	1937	233	.034	367	
4.23	65	.286	1.46	3.28	0.59	18.5	2104	251	.032	346	
4.24	65	.143	1.76	3.28	0.29	18.5	2204	284	.018	273	
4.25	65	.571	0.88	3.28	1.17	18.5	2004	334	.032	252	
4.26	65	.714	0.59	3.28	1.46	19.0	2004	384	.008	189	OCCASIONAL ARCING
4.27	65	.857	0.29	3.28	1.76	19.0	--	-	--	--	
4.28	65	.450	1.13	3.28	0.92	18.5	2271	267	.034	367	
4.29	65	.200	1.64	3.28	0.41	18.5	2071	250	.022	304	
4.30	65	.350	1.32	3.28	0.72	18.5	1937	237	.037	237	REPEAT 4.22
4.31	65	.450	1.13	3.28	0.92	19.0	1238	290	.037	290	REPEAT 4.28

The major result for this test series was that optical pulse energy and peak power increase as corona plate thickness was decreased as shown in Fig. 36 and 37. Although the trend between pulse energy and dielectric thickness is clear, the trend between peak power and dielectric thickness, Fig. 37, shows an anomoly. The 3.0 mm thick dielectric plate gives a greater peak power than the 2.0 mm plate. This behavior could not be explained based upon the data available. Figure 38 is a plot of peak current across the electrode gap for these tests. A clear trend can be observed, the peak current is higher for the 3.0 mm thick plate than for the 1.0 mm plate. Table 10 summarizes peak electron density, input electrical energy and percent of electrical energy expended in producing the UV preionization pulse for the three thicknesses of the dielectric plate. The data has been averaged over the range of N_2/CO_2 investigated.

TABLE 10. EFFECT OF VARYING CORONA PLATE THICKNESS AVERAGED OVER RANGE OF N_2/CO_2

MACOR[R] THICKNESS (MM)	ELECTRON DENSITY (CM^{-3})	INPUT ENERGY (JOULES)	ENERGY IN CORONA PULSE (PERCENT)
1.0	$.88 \times 10^{14}$	1.77	2.1
2.0	1.09×10^{14}	1.89	2.4
3.0	1.34×10^{14}	2.44	2.5

It can be seen that electron density varies from $.88 \times 10^{14}$ to 1.34×10^{14} (follows trend in current) and that from 2.1 to 2.5 percent of the total electrical energy was expended in producing UV preionization.

PRESSURE: 1 ATM
ANODE VOLTAGE: 18.5 KV
CAPACITOR: 10 nF
PRF: 1 PPS
OUTCOUPLING: 82%
APERTURE: 8.5 mm.

CORONA PLATE THICKNESS:
□ - 3.0 mm.
○ - 2.0 mm.
△ - 1.0 mm.

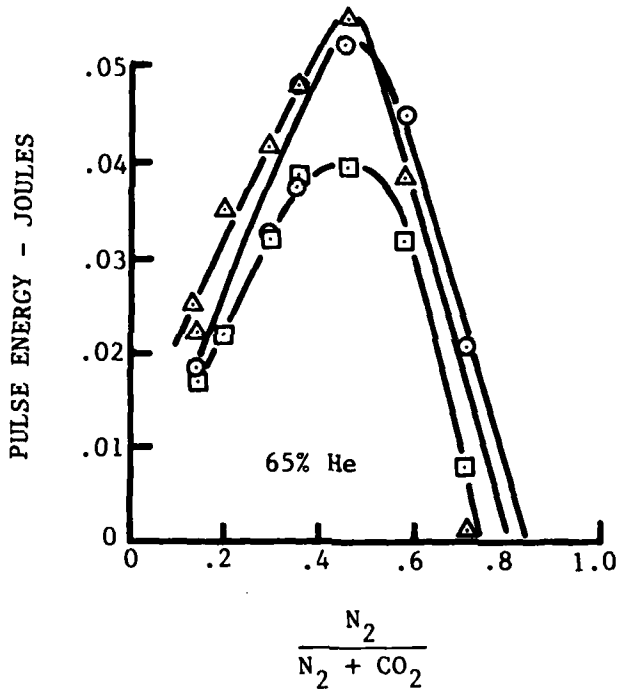

Figure 36. Pulse energy variation for different corona plate thicknesses.

820806010

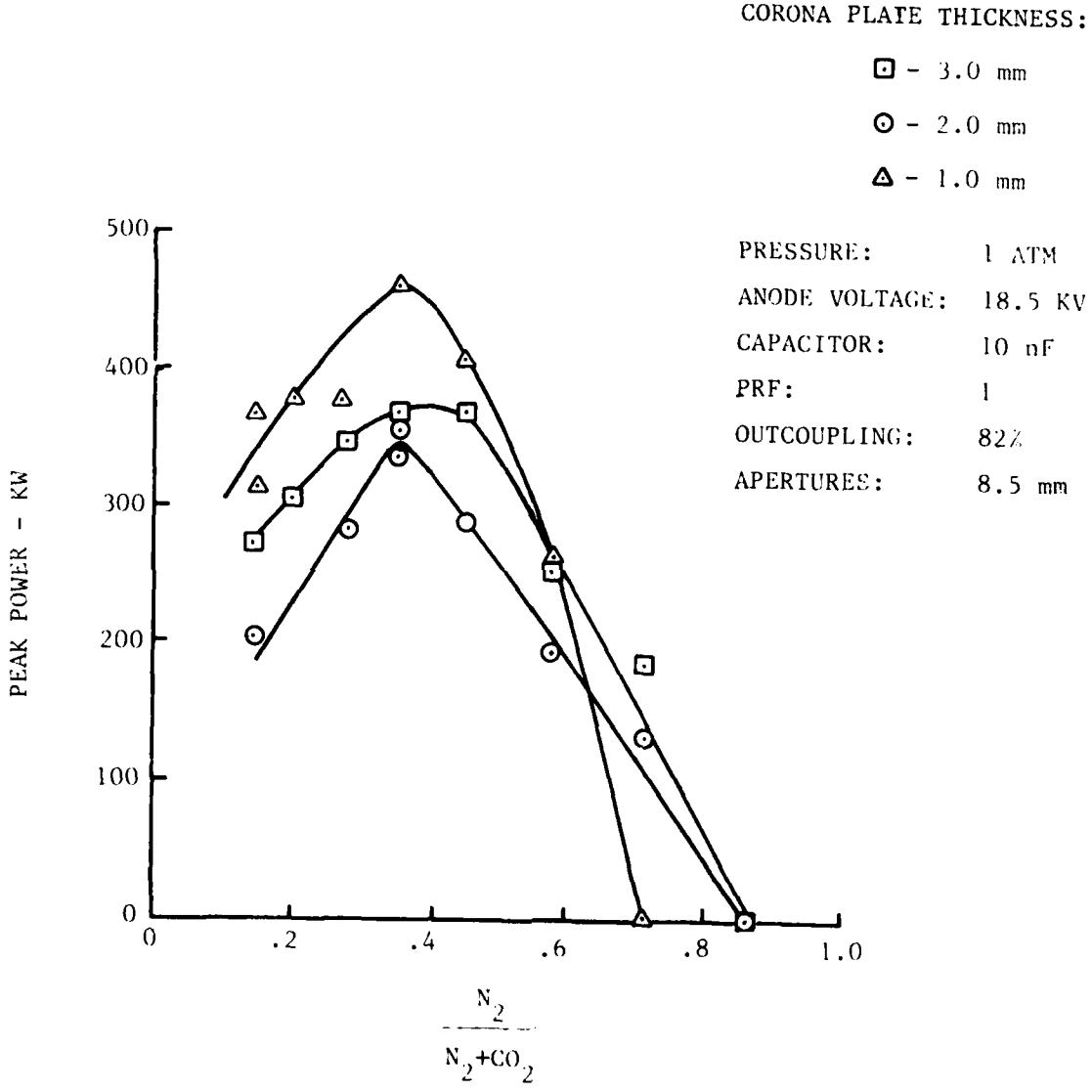

Figure 37. Peak power variation for different corona plate thicknesses.

PRESSURE: 1 ATM
ANODE VOLTAGE: 18.5 KV
CAPACITOR: 10 nF
PRF: 1 PPS
OUTCOUPLING: 82%
APERTURE: 8.5 mm.

CORONA PLATE THICKNESS:

⊡ - 3.0 mm.
⊙ - 2.0 mm.
△ - 1.0 mm.

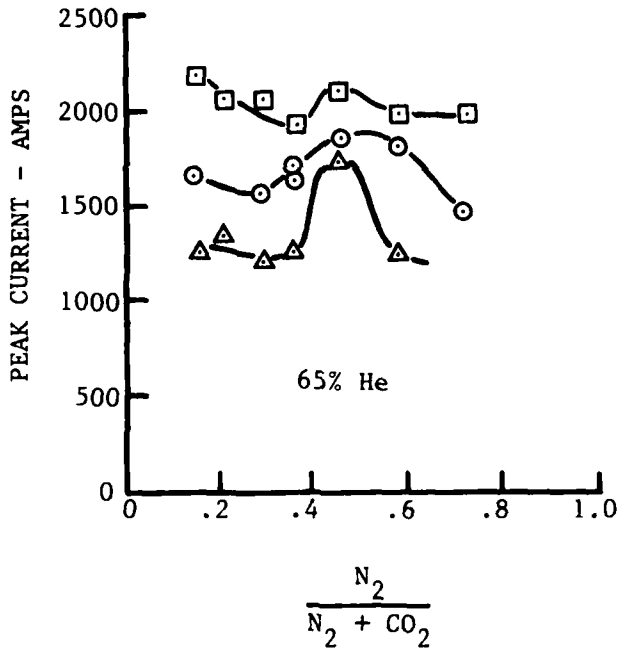

Figure 38. Peak main discharge current for different corona plate thicknesses.

820806009

Results from the corona discharge experiment indicates that UV preionization should be more effective for the thinner 1.0 mm thick dielectric plate. This is due to the fact the the UV light intensity is greater for the thinner plate. Although the efficiency of photoelectron production has not been measured during this investigation, it has been presumed that the higher the UV light intensity, the greater the level of initial electron density. This assumption appears valid since the laser output increased as anticipated for the thinnest dielectric plate. However, the preionization current given in Table 9 does not follow the clear trend established in the corona discharge experiment. In fact, for some compositions, the preionization current for the 3.0 mm thick dielectric plate is greater than for the 1.0 mm plate which is opposite to previous results. The only plausible explanation that can be offered is that the electrical circuit parameters interacted in a more complicated manner than for the well controlled corona discharge experiment.

6.0 CONCLUSIONS AND RECOMMENDATIONS

Conclusions

Although all of the experiments were not completed, enough has been learned to provide some guidelines for the design of a CO_2 TEA laser corona preionizer. To obtain a preionization electron density of 10^5 to 10^8 electrons/cc, it is necessary to maximize the UV photon output from the corona dielectric plates. Uniformity of UV illumination is also important to insure a uniform, high optical quality medium.

Remembering that the time rate of change of current is primarily responsible for the light output, the following guidelines are given.

1. Dielectric materials should be chosen to have the highest combination of dielectric strength and dielectric constant. The desired operating voltage and dielectric strength determine the permissible minimum thickness required. Thicknesses of 1.0 mm produce high UV light output as well as laser performance.
2. The gap between anode and cathode connection should also be minimized consistant with electrode design and main discharge gap height.
3. The distance from the dielectric plates to the electrodes should be minimized to reduce CO_2 absorption of hard UV wavelength light.
4. A symmetrical arrangement of dielectric plates on either side of electrode gap is recommended for uniform illumination.*
5. Avoid operation in the surface sparking regime. Preionization current densities in the 4.0-8.0 amps/cm^2 are recommended for the production of a corona discharge.

---

* This arrangement suits a non-recirculating laser design which was the subject of this research program.

6. Mimimize the helium content in the gas mixture for high laser output. Mixtures of 60-65% or less are desirable.

Recommendations

It is recommended that the experiments not completed in this contract be continued at some future date. Furthermore we recommend that a Faraday charge collector (parallel charge collection plates) be incorporated in the corona discharge experiment and some of the experiments be rerun. The main purpose of the charge collector is to measure the electron density resulting from a beam of UV photons originating at the corona dielectric plate. This measurement would give a direct and measurable result which could be used to assess the effectiveness of the corona preionizer configuration being investigated.

As follow-on work, we recommend the mathematical modeling of the corona preionization process so that it could be incorporatied into an existing UTRC CO_2 pulsed laser computer code. The corona preionization model would generate the electron density pulse based upon modeling the process and would serve as the initial condition for the laser code. The model will predict electron and positive-ion densities and current and voltage waveform. It would allow the optimization of a corona preionized laser design to be assessed in terms of laser output parameters.

7.0 REFERENCES

1. Ernst, G. J.: Single-Frequency, Atmospheric Pressure CO_2 Laser. Rev. Sci. Instrum., Vol. 48, No. 10, October 1977.
2. Ernst, G. J., snd A. G. Boer: Construction and Performance Characteristics of a Rapid Discharge TEA CO_2 Laser. Optics Communications, Vol. 27, No. 1, October 1978.
3. Brink, D. J. and V. Hason, High-Power Photopreionization-Stabilized Carbon Dioxide Waveguide Lasers Operating ast Gas Pressures of up to 13 atm, J. Appl. Phys., 49 (4), April 1978.
4. Hasson, V and H. M. Von Bergman, Ultraminiture High-Power Gas Discharge Lasers, Rev. Sci., Instrum., Vol. 50, No. 1, January 1979.
5. Von Bergmann, H. M., Sealed-Off, Miniature, High-Power Nitrogen, Laser, J. Phys. E 10, 1210, May 1977.
6. Von Bergmann, H. M. and V. Hasson, High Pressure Glow discharges for Nanosecond Excitation of gas Lasers and Low Inductance Switching Applications, J. of Physics E: Scientific Instruments, 1976, Vol. 9, Great Britain, 1976.
7. Meek, J. M., and J. D. Craggs: Electrical Breakdown of Gases. Oxford University Press, Great Britain, 1953.
8. Hirsch, M. N., and H. J. Oskam: Gaseous Electronics, Vol. 1, Electrical Discharges. Academic Press, NY, 1978.
9. Beverly, R. E. III: Light Emission from High - Current Surface - Spark Discharges, Chapter VI, Progress In Optics XVI, E. Wolf editor, North Holland, 1978.
10. Tallman, C. R.: A Study of Excimer Laser Scientific Laboratory Preionization Techniques, LA-UR 79:1630, Los Alamos Paper presented at the Optical Society of America, Excimer Laser Meeting.

11. Baranov, V. Yu: Use of a Discharge Over a Dielectric Surface for Preionization in Excimer Lasers, Society Journal Quantum Electronics, 11(1), Jan. 1981.

12. Chang, T.Y.: Improved Uniform - Field Electrode Profiles for TEA Laser and High Voltage Applications, Rev. Sci. Instr., 44(1973) 405.

13. Pace, P.W. and Marc Lacombe: A Sealed High-Repetition-Rate TEA CO_2 Laser, IEEE, Journal of Qunatum Electronics, Vol. QE-14, No. 4, April 1978. 14.

14. McKen, D. C., H. J. Sequin, and J. Tulip: Photoionization Parameters in the Carbon Dioxide Laser Gases. IEEE Journal of Quantum Electronics, Vol. QE-12 No. 8, August 1976.

15. Heald, M. A., and C. B. Wharton: Plasma Diagnostics With Microwave. John Wiley and Sons, Inc., NY, 1965.

16. Seguin, H. J., J. Tulip and D. C. McKen: Ultraviolet Photoionization in TEA Lasers. IEEE Journal of Quantum Electronics, P. 311-319, Vol. QE-10, No. 3, March 1974.

17. Babcock, R. V., I. Liberman, and W. D. Partlow: Volume Ultraviolet Preionization From Bare Sparks. IEEE Journal of Quantum Electronics, Vol. QE-12, No. 1, January 1976.

APPENDIX A - PHOTOIONIZATION OF PULSED TEA LASERS

Background

Photoionization of electrically pulsed, CO_2 lasers has proven to be a very efficient technique of introducing initiating electrons in the main electrode gap. The end result is a very volume efficient, high peak power and narrow pulse width laser[A1,A2,A3]. The discussion of the basic mechanisms involved was taken from Meek and Craggs[A4] and presented in the following paragraphs

The time lage between the application of an impulse voltage and the consequent breakdown of a gap can be separated into two components:

$$\tau = \tau_s + \tau_f \qquad \text{(A-1)}$$

where,

τ_s: The statistical time lag is caused by the need for an electron to appear in the gap during the period of application of the voltage in order to initiate the discharge,

τ_f: The formative time lag corresponds to the time required for the discharge, once initiated, to develop across the gap.

The statistical time lag depends upon the amount of pre-ionization or irradiation of the discharge gap. A gap subjected to an impulse voltage may breakdown if the peak voltage reaches the DC breakdown value, provided that the gap is sufficiently irradiated so that an electron is present to initiate the discharge process. With a lower amount of irradiation, the voltage must be maintained above the D.C. breakdown value for a longer period before an electron appears.

According to Hirsch[A5], the formative time lag (τ_f) plays a negligible role in the measured time lag (τ). For small distances (1 cm), estimates for τ_f are smaller than 10^{-9} sec, compared to measured time lags in the 10^{-8} to 10^{-6} sec range.

The fact that irradiation reduces the statistical time lag has long been known (since the mid 1920's acording to references given in Meeks and Scrags, Ref. 4). The various sources of irradiation that have been used included radioactive materials, x-rays, and ultraviolet illumination provided by a suitable arc-lamp or by spark or corona discharge. With respect to small, electrically pulsed CO_2 TEA lasers, the spark discharge method of producing U.V. illumination has been most popular and successful[A1 A2 A6 A7 A8]. The physics involved is well understood and backed by a great deal of physical measurements. Analytical models[A9 A10] have also been developed which agree reasonable well with experimental data. The spark discharge method serve as a convenient starting point for the research presented in this report. The methodology and measurements techniques were directly applicable with minor changes to corona discharge investigations.

Preionization Requirements for Initiating Glow Discharges

While application of UV photoionization in pulsed TEA lasers has become common, it is worthwhile to review the basic physics of the gap conditioning mechanism. This will help in understanding the requirements that must be imposed upon the surface corona preionizer. The streamer theory of gap breakdown is most applicable to electrically pulsed TEA lasers. Palmer[A11] was the first investigator to report results of theoretical work to predict preioniation requirements for a pulsed CO_2 TEA laser. More recently Levatter and Lin[A12] extended Palmers model to included a number of important effects which were neglected by Palmer. The material presented in this Appendix has been extracted from Meek and Craggs book as well a from Palmer's paper. Palmer's theory is simple and does explain the physics quite clearly. At the conclusion of this Appendix, a discussion of the Palmer model's shortcommings is presented along with Levatter and Lin's contributions.

Palmer's model is based on consideration of individual electron avalanches, the transition from an avalanche into a streamer, and the mechanism of advance of streamers. The theory involves ionization processes dependent upon the gas only, including ionization by electron collision according to the Townsend α-mechanism, photoionization and space-charge field effects caused by avalances and streamers. Initially, consider the application of a voltage gradient of, E, volts per cm. across a gap of length, d, cm. between parallel plane electrodes in a gas at a presssure of, p, mm Hg in the absence of preionization. If the ratio, E/p, is sufficiently high, an electron leaving the cathode will ionize the gas molecules, and the additional electrons so formed will also be accelerated in the applied field and cause further ionization. When the original electron has moved a distance, x, in the direction of the applied field, the number of electrons create' is e^x. The process is rapidly cumulative, and is appropriately termed an electron avalanche. In a field with the magnitude requred to cause breakdown, the electrons travel at a speed of the order of 2×10^7 cm/sec, while the positive ions from which the electrons have been detached have a speed of about 2×10^5 cm/sec. The positive ions may therefore be considered stationary in comparison with the more rapidly moving electrons, and the avalanche develops across the gap as a cloud of electrons behind which is left a positive ion space charge, in the manner indicated in Fig. A-1(a).

The space charge produced by the electron avalanche produces a distortion of the field in the gap, as shown in Fig. A-1(a). The distortion is greatest in the region of the head of the avalanche, where the ion density reaches its highest value. The space-charge field, E_r, augments the externally applied field, E, and also creates a field in the direction radial to the axis. It is assumed that when $E_r = KE$, then the space-charge field increases the magnitude of the field along the axis to a maximum value of $(1 + K)E$.

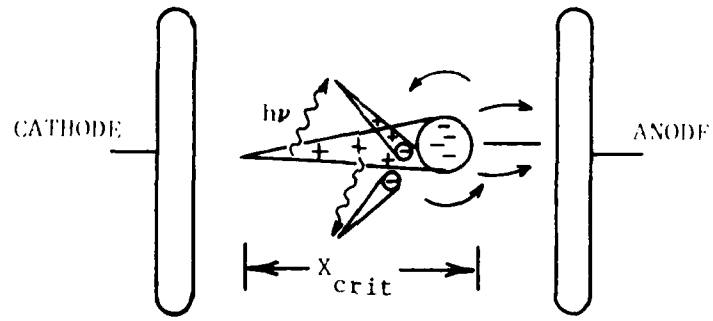

(a)

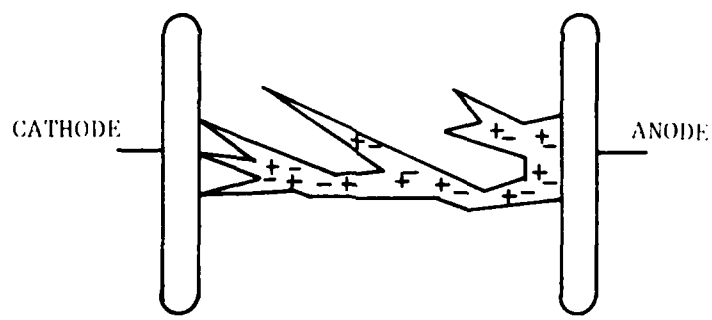

(b)

Figure A-1. Streamer breakdown initiated by a single primary avalanche: (a) initial, (b) final charge distributions.

The electrons in the gas surrounding the avalanche, are produced by photons emitted from the densely ionized gas constituting the avalanche stem. These electrons initiate auxiliary avalanches which, if the space-charge field developed by the main avalanche is of the order of the external field, will be directed towards the stem of the main avalanche. The greatest multiplication in these auxillary avalanches will occur along the axis of the main avalanche where the space-charge field supplements the external field. Positive ions left behind by these avalanches effectively lengthen and intensify the space charge of the main avalanche in the direction of the cathode, and the process develops as a self-propagating streamer, shown in Fig. A-2(b). The streamer proceeds across the gap to form a conducting filament of highly ionized gas between the electrodes. This filament constitutes the initial stage of the spark channel through which the external circuit discharges.

The transition from an electron avalanche into a streamer is considered to occur when the radial field, E_r, produced by the postive ions at the head of the avalanche is of the order of the externally applied field E. Unless this is so, there will be no appreciable enhancement of ionization in the region of the avalanche or division of subsidiary electron avalanches to the main avalanche. Since the applied field E is related to the product of pd, the condition is commonly known as Reather's breakdown criterion and is given by Eq. (A-2) for air. α is known as the first Townsend ionization coefficient.

$$(\alpha/p)\ pd = 20 + \ln d \qquad \text{(A-2)}$$

The streamer breakdown criterion given by Eq. A-2 is easily satisfied for a typical TEA laser discharge. Clearly such a breakdown mechanism, if allowed to progress in the normal manner described above, will do so for an arc mode rather than the desired glow mode initiation of the discharge.

AD-A122 552 CORONA PREIONIZATION TECHNIQUE FOR CARBON DIOXIDE TEA LASERS(U) UNITED TECHNOLOGIES RESEARCH CENTER WEST PALM BEACH FL OPTICS.. W R KAMINSKI 30 NOV 82 2/2

UNCLASSIFIED UTRC/82R-980701-02 DAAK70-81-C-0077 F/G 20/5 NL

END

FILMED

DTIC

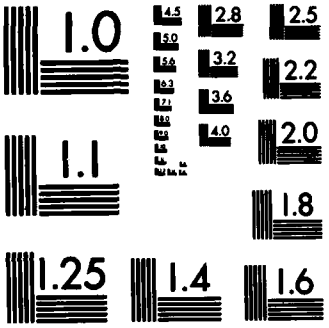

MICROCOPY RESOLUTION TEST CHART
NATIONAL BUREAU OF STANDARDS-1963-A

How does preionization alter the situation so far described? To best answer this question, it is first necessary to briefly review the derivation of the streamer breakdown criterion given by Eq. (A-2).

The lateral extent (perpendicular to the field direction) of an individual avalanche is usually assumed to be due to diffusion, although electrostatic repulsion may be comparable in some cases. In the case of diffusion, it can easily be shown that:

$$r^2 = x l_m \qquad \text{(A-3)}$$

where r is the radius of the head of an avalanche after it has propagated a distance x in the field direction, and l_m is the electron mean free path. One calculates the space-charge field, E_r, of the avalanche by assuming that all of the electrons in the avalanche, N_e, are concentrated in the head of the avalanche which is assumed spherical with radius r. One writes, therefore,

$$E_r = eN_e/4 \quad \varepsilon_o r^2 \qquad \text{(A-4)}$$

where e is the electron charge, ε_o is the free-space permittivity, and N_e is given by the Townsend avalanche condition:

$$N_e = \exp(\alpha x). \qquad \text{(A-5)}$$

Equating the space-charge field at the surface of the avalanche head to the applied field E_o by using Eqs. (A-3) to (A-5) gives a formula for the critical distance x_{crit}, which an individual avalanche must propagate to initiate streamer breakdown.

$$\alpha x_{crit} = \ln(4\pi\varepsilon_o E_o l_m/e) + \ln x_{crit} \qquad \text{(A-6)}$$

The first term in the right side is fairly insensitive to the gas parameters and is about 20 in mks units for typical breakdown conditions. Equating x_{crit} to the gap spacing, d, gives Reather's criterion, Eq. (A-2).

Now the above criterion for streamer formation contains no dependence on the initial (preionized) electron density. What is also important for streamer formation, but is not explicitly stated in Eq. (A-6), is that the space-charge field

has an appreciable local gradient since it is this feature which causes the ionization to become filimentary. In the case where the space-charge field is due to a single primary avalanche as assumed for the derivation of Eq. (A-6), such a local gradient clearly exists. However, as the density of primary avalanches is increased, the field gradient associated with the avalanche space charge fields can be expected to become sufficiently uniform to eliminate the tendency of the secondary avalanches to converge towards a single primary avalanche [Fig. A-2(a)]. Let n_o represent the density of primary avalanches (preionization electron density). The ratio $(n_o d)^{-1/3}/r$ can then be taken as a measure of the smoothness of the avalanche space-charge fields, where r is the lateral extent of the avalanche [Eq. (A-1)] and $(n_o)^{-1/3}$ is the average lateral separation of the avalanches. It is reasonable to assume that filamentary streamer formation will be suppressed in a favor of a more uniform space-charge-controlled ionization stage which can initiate a uniform glow discharge when the value of this ratio becomes less than or comparable to unity at the critical stage when space-charge field become comparable to the applied field [Fig. A-2(b)]. This condition can be written, using Eq. (A-3), as

$$(n_o)^{-1/3} < (l_m x_{crit})^{1/2}, \qquad \text{(A-7)}$$

with x_{crit} given by Eq (A-6).

Typical parameters for CO_2 TEA breakdown conditions are $l_m \approx 10^{-3}$ cm, $\alpha \approx 10$ cm^{-1}. For these values, Eqs. (A-7) and (A-6) require, for glow mode initiation,

$$n_o > 10^4 \text{ cm}^{-3} \qquad \text{(A-8)}$$

Note that to first order, n_o varies with the cube of the pressure (for fixed E/p). Another condition which must be satisfied in order to produce glow discharge is that the gap must be preionized uniformly in a plane parallel to the electrodes. The above threshold preionization density is consistent, in order of magnitude, with experimental observations. These measurements will be discussed in Section 2.

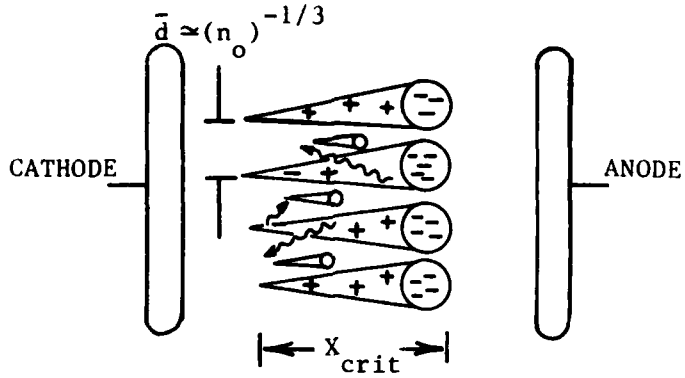

(a)

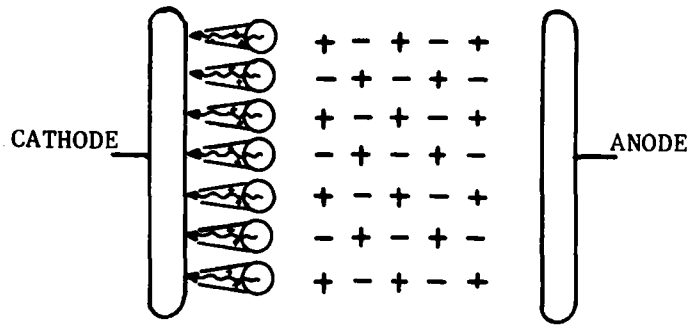

(b)

Figure A-2. Preionized breakdown initiated by multiple primary avalanches: (a) initial, (b) final charge distributions.

820806026

While the physical model as proposed by Palmer[11] was basically sound, there appeared to be two serious deficiencies in his subsequent formulation according to Levatter and Lin[12]. The first was the neglect of the important effects of a finite voltage rise time on the depletion of free electrons (preionization electrons) near the cathode during the preavalanche period, and the neglect of those effects on the subsequent development of the electron avalanche process. The second was the absence of any explicit functional relationship between such important physical properties of the gas mixture as the first Townsend coefficient, the electron mobility, and the applied electric field strength to gas density ratio E/n throughout the formulation. In addition, a sizable error was made in relating the electron diffusion radius to the electron mean-free path and the drift distance.

Levatter and Lin's analysis is beyond the scope of this Appendix however, the net result of their analysis shows that the minimum preionization density is from 1 to 2 orders of magnitude greater than that predicted by Palmer. Thus for CO_2 TEA lasers, the minimum preionization density required is from 10^5 to 10^6 electrons/cc depending upon specific conditions.

REFERENCES FOR APPENDIX A

A1. Stark, D. S., P. H. Cross, and H. Foster: A Compact Sealed Pulsed CO_2 TEA Laser. IEEE Journal of Quantum Electronics, Vol. QE-11, No. 9, September 1975.

A2. Stark, D. S., P. H. Cross, and M. R. Harris: A Sealed UV-Preionization CO_2 TEA Laser With High Peak Power Output. J. Phys. E: Sci. Instrum., Vol. 11. Printed in Great Britian, 1978.

A3. Ernst, G. J., and A. G. Boer: Construction and Performance Characteristics of a Rapid Discharge TEA CO_2 Laser. Optics Communications, Vol. 27, No. 1, October 1978.

A4. Meek, J. M. and J. D. Craggs: Electrical Breakdown of Gases. Oxford University Press, Great Britain, 1953.

A5. Hirsh, M. N., and H. J. Oskam: Gaseous Electronics, Vol. 1, Electrical Discharges. Academic Press, NY, 1978.

A6. Memjuk, N., and P. F. Moulton: Development of a High-Repetition-Rate Mini-TEA CO_2 Laser. Rev. Sci. Instrum. 51(2), February 1980.

A7. Yamabe, C., T. Matsushita, S. Sato, and K. Horii: Parametric Studies of UV Preionization in TEA CO_2 Lasers. J. Appl. Phys. 51(2), Februray 1980.

A8. Lambertson, H. M., and P. R. Pearson: Atmospheric Pressure CO_2 Lasers Giving High Output Energy Per Unit Volume. IEEE J. of Quantum Electronics, Vol. QE-8, No. 2, Februrary 1972.

A9. Kline, L. E., and L. J. Denes: Investigations of Glow Discharge Formation With Volume Preionization. J. of Appl. Phys., Vol. 46, No. 4, April 1975.

A10. Palmer, A. J., W. M. Clark, and J. Y. Wada: Ultraviolet Preionized CO_2 Laser Research. Hughes Research Laboratories, Sponsored by USAF Weapons Laboratory, Contract No. F29601-73-C-0107, Report AFWL-TR-74-107 (ADB003904), March 1975.

A11. Palmer, A. J.: A Physical Model on the Imitation of Atmospheric-Pressure Glow Discharges. Applied Phys. Letters, Vol. 25, No. 3, August 1, 1974.

A12. Levatter, J. I. and Shao - Chi Lin: Necessary Conditions for the Homogeneous Formation of Pulsed Avalanche Discharges of High Gas Pressures, J. Appl. Phys. 51(1), January (1980).

APPENDIX B - DESIGN OF EXPERIMENTAL APPARATUS

This Appendix presents design details of the major test hardware which was fabricated for use in this contract. Reduced copies of the main layout drawings are included to assist the descriptions given.

Corona Discharge Apparatus

As discussed in Section 4.0 of this report, the purpose of this test apparatus was to provide an isolated section of the corona dielectric plate and corresponding electrodes which reproduces the physical conditions occuring in the TEA laser durng preionization. The model of the corona dielectric plate is then enclosed in a vacuum tight chamber having suitable connections (electrical and filling) and attachments for direct mounting to a vacuum monochromator.

The following features were considered during the design of the experimental apparatus.

1. The corona dielectric plate and electrodes must be attached to a dielectric carrier which allows for variable gap between electrodes and allows the entire unit to be translated acrosss the monochromator entrance slit.
2. Variable plate thickness and different dielectric materials must be accomodated.
3. The corona plate to LiF window distance must be typical of the width-wise dimension in the laser (approx. 3.5 cm).
4. The corona experimental chamber must be vacuum tight and made from a dielectric such a Pyrex. An inlet and outlet flow port and pressure tap must be provided as well as a port for aligning the system.
5. EMI shielding must be provided around entire corona chamber.
6. Ease of hardware installation and rapid changes in configuration must be accomodated.

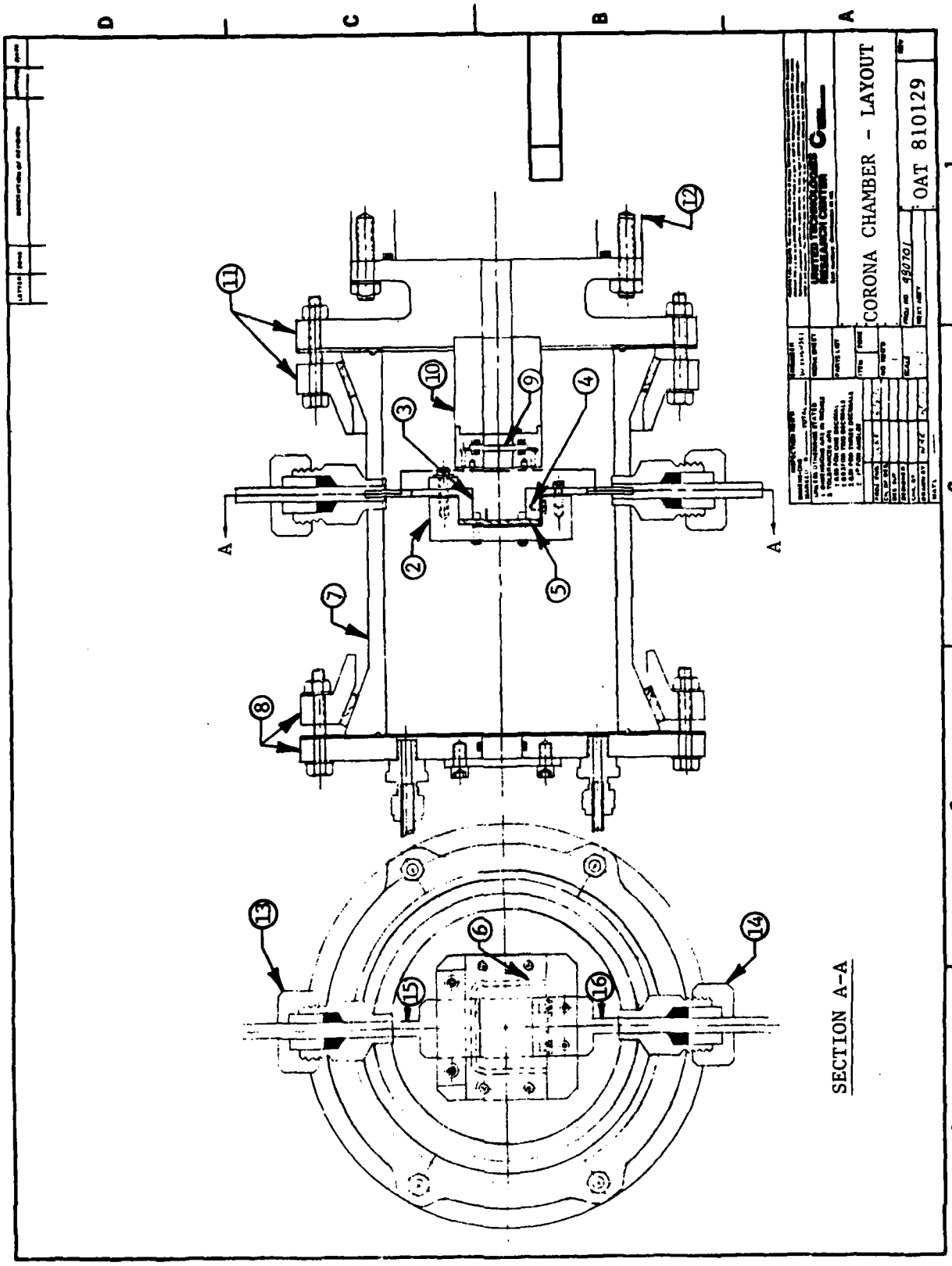

Figure B-1. Layout drawing of corona discharge experimental apparatus.

7. The corona chamber must mate directly to the monochromator without interfering with the detector.

The above considerations led to the design shown in Fig. B-1 which is a layout drawing of the corona discharge apparatus. A nominal 2.54 cm wide by 2.03 cm high section of the CO_2 TEA laser preionizer was selected as a model. The corona dielectric plate, item (1) in Fig. A-1, is approximately 7.6 cm wide by 5.1 cm high and is attached to a MACOR carrier (2). An anode (3), a cathode (4) and a ground plane or cathode extension (5) are all made of copper and are 2.54 cm wide. The copper ground plane (5) is in intimate contact with the back surface corona dielectric plate and sets the 2.54 cm width condition. The height of the corona plate depends upon the gap between the anode and cathode. An o-ring (6) made from silicon and compressed between the corona plate and carrier is used to hold-off the voltage potential between the ground plane (5) and the anode (3). The entire assembly is suspended in a Pyrex glass pipe (7) by compressing the anode and cathode leads (15) and (16) in a pair of Conax fittings (13) and (14). These fittings also assure sealing tightness. The Pyrex pipe (6) is clamped between 2 pairs of flanges (8) and (11) which form the corona chamber. A LiF window (9) is held in a pressure/vacuum sealing mount (10). The distance from the LiF window and the corona dielectric plate is 3.05 cm which is approximately the width of our electrodes in the TEA laser. An approximately 3.8 cm long MACOR standoff prevents arcing from the anode to the window holder and ultimately to the flange (11). Flange (11) also serves as the adapter between the corona chamber and entrance slit to the vacuum monochromator.

Figure B-2 shows the electrical circuit components and EMI shielding of the corona chamber. A brass cylinder, item (1) in Figure B-2, covers the entire Pyrex glass pipe from flange to flange to provide EMI shielding. The anode lead is connected to a brass disc (3) which can slide in a slotted brass cylinder

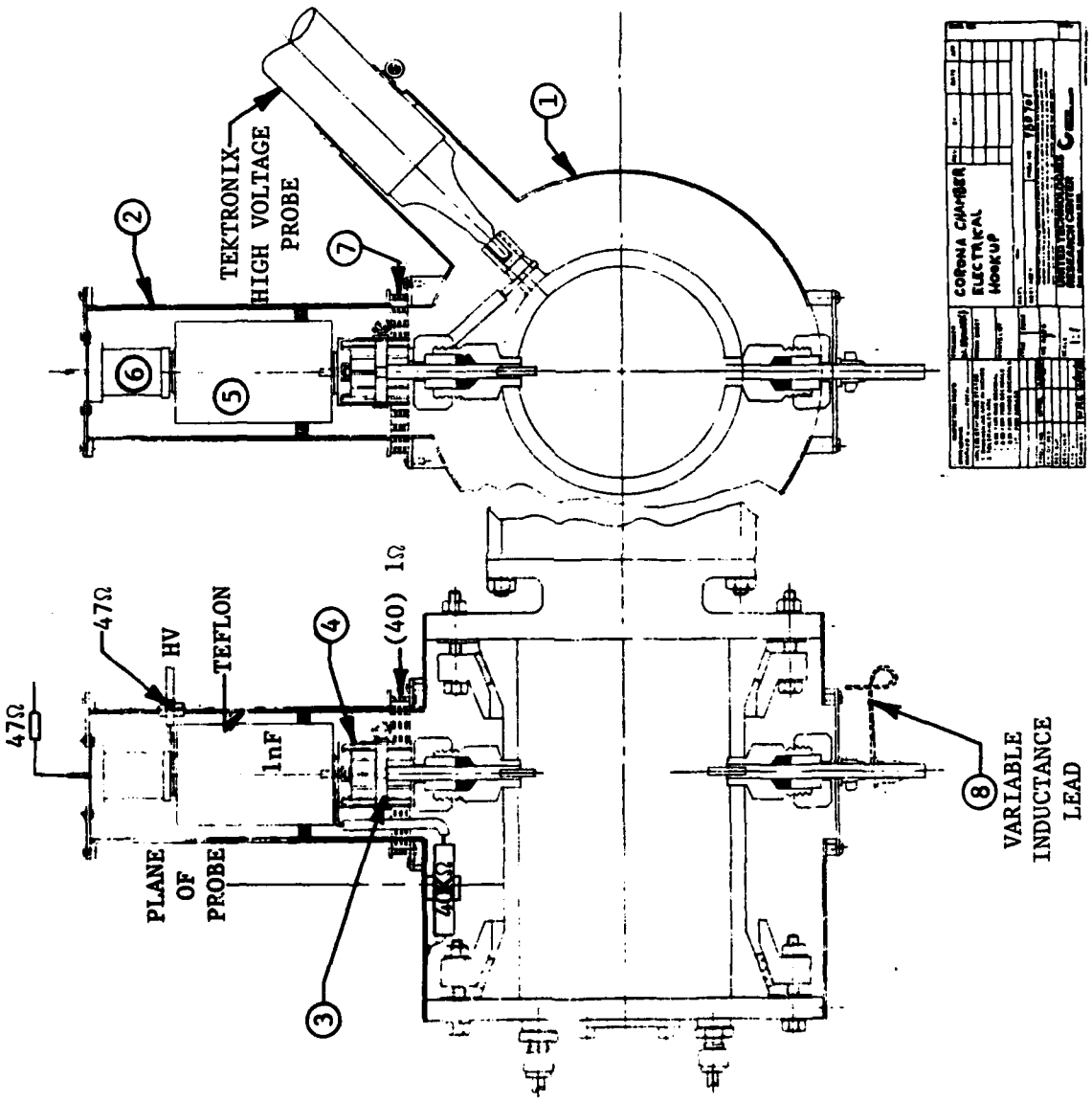

Figure B-2. Electrical circuit components and EMI shielding of corona chamber.

7. The corona chamber must mate directly to the monochromator without interfering with the detector.

The above considerations led to the design shown in Fig. B-1 which is a layout drawing of the corona discharge apparatus. A nominal 2.54 cm wide by 2.03 cm high section of the CO_2 TEA laser preionizer was selected as a model. The corona dielectric plate, item (1) in Fig. A-1, is approximately 7.6 cm wide by 5.1 cm high and is attached to a MACOR carrier (2). An anode (3), a cathode (4) and a ground plane or cathode extension (5) are all made of copper and are 2.54 cm wide. The copper ground plane (5) is in intimate contact with the back surface corona dielectric plate and sets the 2.54 cm width condition. The height of the corona plate depends upon the gap between the anode and cathode. An o-ring (6) made from silicon and compressed between the corona plate and carrier is used to hold-off the voltage potential between the ground plane (5) and the anode (3). The entire assembly is suspended in a Pyrex glass pipe (7) by compressing the anode and cathode leads (15) and (16) in a pair of Conax fittings (13) and (14). These fittings also assure sealing tightness. The Pyrex pipe (6) is clamped between 2 pairs of flanges (8) and (11) which form the corona chamber. A LiF window (9) is held in a pressure/vacuum sealing mount (10). The distance from the LiF window and the corona dielectric plate is 3.05 cm which is approximately the width of our electrodes in the TEA laser. An approximately 3.8 cm long MACOR standoff prevents arcing from the anode to the window holder and ultimately to the flange (11). Flange (11) also serves as the adapter between the corona chamber and entrance slit to the vacuum monochromator.

Figure B-2 shows the electrical circuit components and EMI shielding of the corona chamber. A brass cylinder, item (1) in Figure B-2, covers the entire Pyrex glass pipe from flange to flange to provide EMI shielding. The anode lead is connected to a brass disc (3) which can slide in a slotted brass cylinder

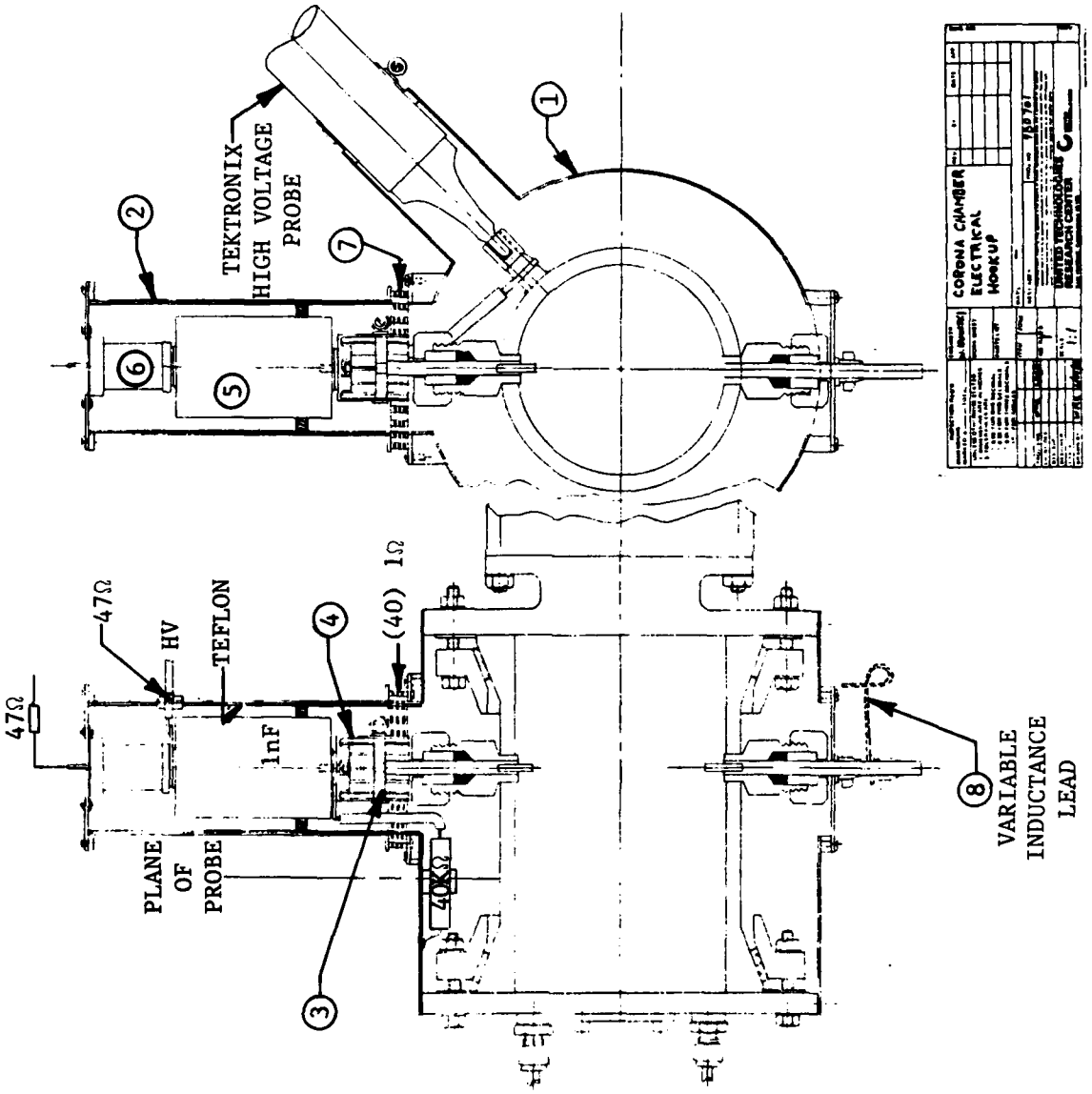

Figure B-2. Electrical circuit components and EMI shielding of corona chamber.

(4). Contact is maintained by employing a band clamp. Cylinder (4) is connected to a 1 n-Farad capacitor (5) which in turn is connected to a 24 KV, EG&G type GP-96-24 spark gap (6). These circuit components are arranged in a

linear manner to reduce circuit inductance and produce high efficiency coupling into the corona plate. The electrical components are housed in an EMI shielding cylinder (2) which is teflon lined to prevent internal arcing. The circuit is attached to ground at the bottom of the EMI housing where the cathode is locked into a cover plate. To vary circuit inductance, a variable length wire is added (8) to give the desired additional circuit inductance. Provisions are made to house a Tektronix high voltage probe for measuring the anode voltage pulse. Forty, 1Ω resistors are mounted in parallel between the electrical component cylindrical housing and main EMI shield. These resistors serve as a shunt for reading current passing through the corona plate when conduction takes place following a voltage pulse.

Figure B-3 shows a simplified circuit diagram of the Corona discharge experiment electrical system driven by a negative high voltage power supply. It is self explanatory and will not be discussed further.

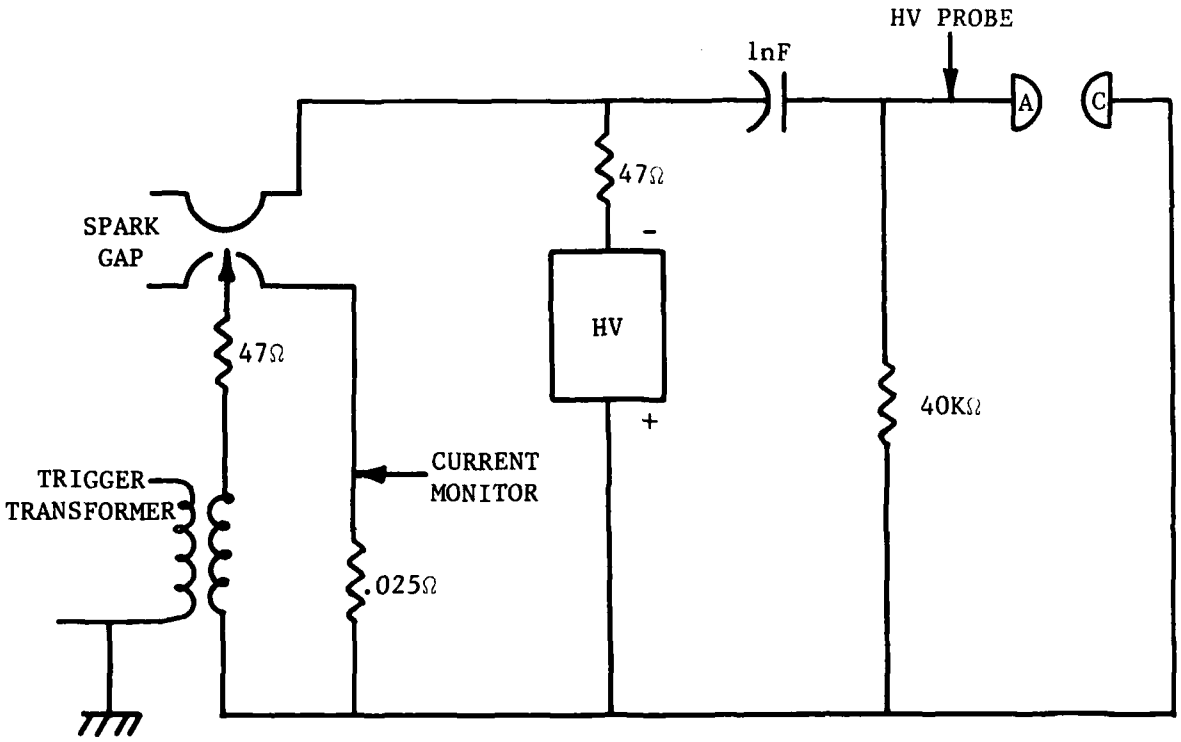

Figure B-3. Electrical system schematic for corona discharge experiment.

APPENDIX C - DIELECTRIC MICROWAVE ANTENNA

Although results from the microwave interferometry experiment using an X-band microwave source proved to be inconclusive, the design of a dielectric antenna to introduce the radiation into a laser cavity was very successful. The antenna had excellent directional properties and low energy loss. Therefore it is felt that the presentation of design methodology for such an antenna is very useful and will be outlined in this appendix.

The basic idea is to insert a dielectric material into a rectangular microwave waveguide and shaping the leading edge such that all radiation entering the dielectric is internally reflected in the forward direction. The trailing edge of the dielectric is shaped such that the radiation internally reflected from the leading edge can emerge with a minimum of divergence from the centerline.

The derivation of the design equation follows from the definition of geometric variables shown in Fig. C-1. Let a be the long side and b the short side of a metallic waveguide. The propagation angle of an EM wave in the guide is,

$$\theta_G = \arctan\left[\frac{1}{2a}\cdot\frac{\lambda}{\sqrt{1-(\lambda/2a)^2}}\right] \qquad \text{(C-1)}$$

where λ is the wavelength of the microwave radiation.

Without discussion, the various geometric parameters are given by equations (C-2) through (C-11). The index of refraction of the medium in the waveguide is $n = 1$ and for the dielectric is n'.

$$\theta_i = 90 - (\theta_D + \theta_G) \qquad \text{(C-2)}$$

$$\theta_i = \arcsin\left[\frac{n}{n'}\cdot\sin\theta_i\right] \qquad \text{(C-3)}$$

$$\beta = 90 - \alpha = 90 - 2\,\theta_D \qquad \text{(C-4)}$$

$$\theta''_i = 2\,\theta_D + \arcsin\left\{\frac{n}{n'}\sin\left[90-(\theta_D+\theta_G)\right]\right\} \qquad \text{(C-5)}$$

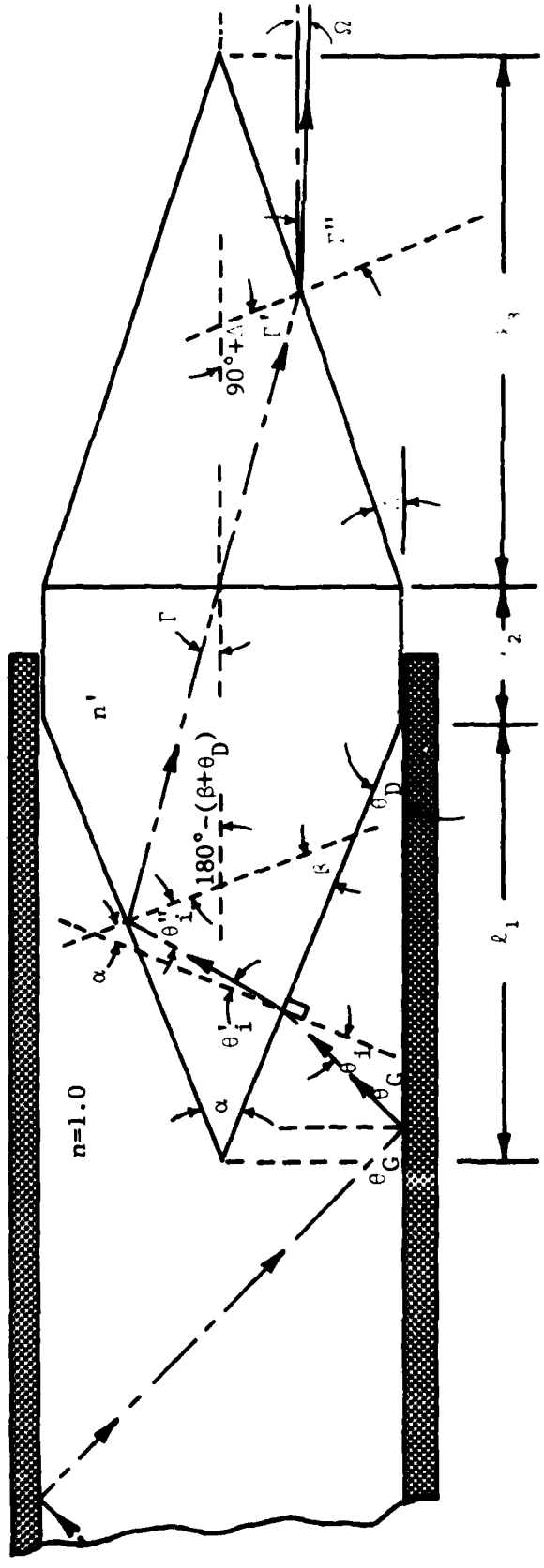

Figure C-1. Geometry for design of dielectric microwave antenna.

820806002

Note that for total internal reflection $\theta''_1 > \arcsin \frac{1}{n'}$,

$$\Gamma = \beta + \theta_D - \theta''_1 \qquad \text{(C-6)}$$

$$\Gamma = 90 - (\Gamma + \Delta) \qquad \text{(C-7)}$$

Also note that to prevent total internal reflection, $\Gamma' < \arcsin \frac{1}{n'}$.

$$\Gamma'' = \arcsin \left[\frac{n'}{n}, \sin \right] \qquad \text{(C-8)}$$

$$\Gamma'' = \arcsin \left[\frac{n'}{n}, \sin \left\{ 3\Theta_D + \arcsin \left[\frac{n}{n'} \cdot \sin (90 - \Theta_D - \Theta_G) \right] - \Delta \right\} \right] \qquad \text{(C-9)}$$

$$\Omega = (90 - \Delta) - \Gamma'' \qquad \text{(C-10)}$$

Finally substituting (C-9) into (C-10) gives the design equation.

$$\Omega = (90 - \Delta) - \arcsin \left[\frac{n'}{n} \cdot \sin \left\{ 3\Theta_D + \arcsin \left[\frac{n}{n'} \sin (90' - \Theta_D - \Theta_G) \right] - \Delta \right\} \right] \qquad \text{(C-11)}$$

where, Ω is ( ) for a converging wave.

Ω is (+) for a deverging wave.

Polystyrene with $n' = 1.60$ was chosen for our antenna design. Figure C-2 gives the design details for the antenna. Note that for this design $l_2 = 0$, $a = 22$ and $\Delta = 49.6^\circ$. If the microwave source is operated at 10.3 GHz then $\lambda =$ 2.9 cm. An RG-52 waveguide has a dimension of 2.286 cm. The propagation angle of the EM wave in the guide is $\theta = 39.37^\circ$. For these parameters $\Omega = 29.3^\circ$.

At first glance one might question the directional quality of this antenna with an $\Omega = 29.3^\circ$. However, test results show that the directional characteristics of this antenna are good as shown in Fig. C-3. The frequency response of waveguide and connected to a TEA laser cavity is shown in Fig. C-4. As shown, the frequency response is rather flat in the 9.5 to 10.5 GHz range of interest.

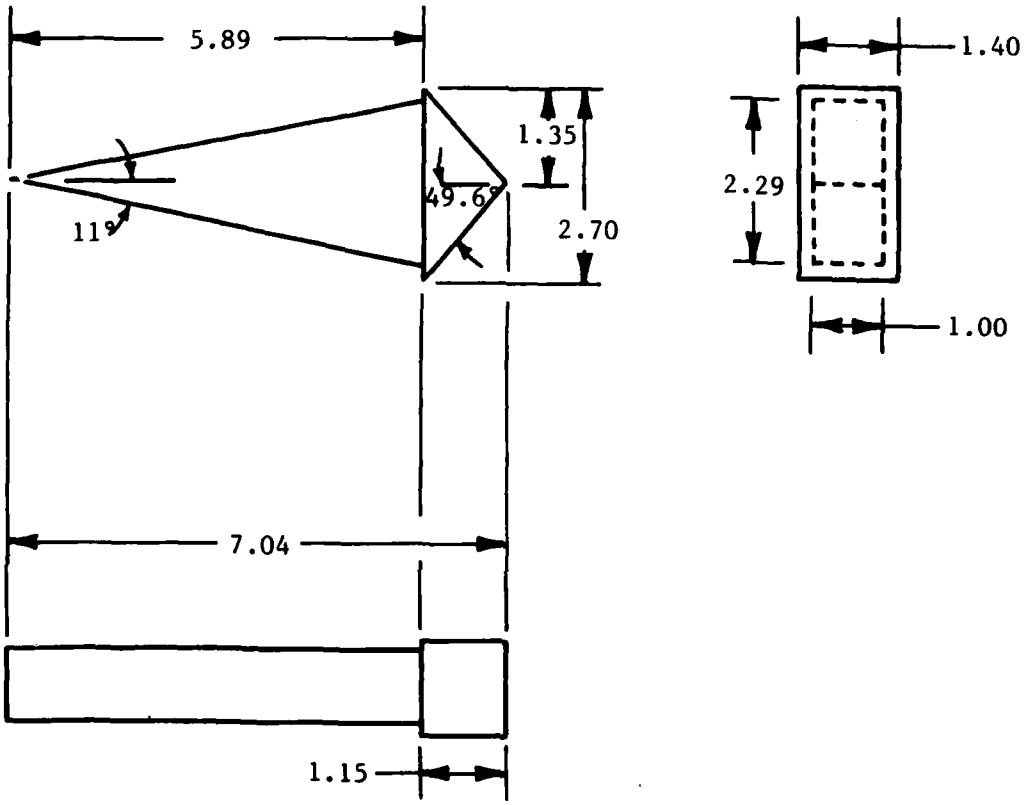

NOTES:

1. ALL DIMENSIONS IN CENTIMETERS
2. MATERIAL: POLYSTYRENE PLASTIC
3. TOLERENCE: LINEAR DIMENSIONS ±0.05 CM.

Figure C-2. Polystyrene plastic microwave antenna design.

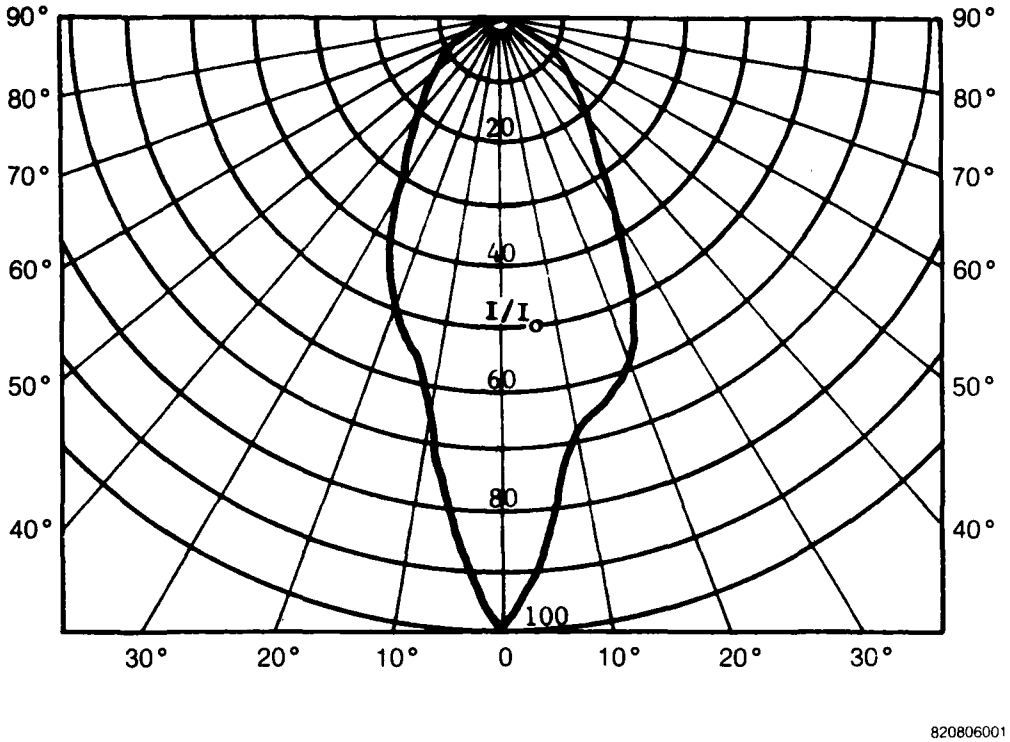

Figure C-3. Directional characteristics of a polystryene microwave antenna at 10 GHz.

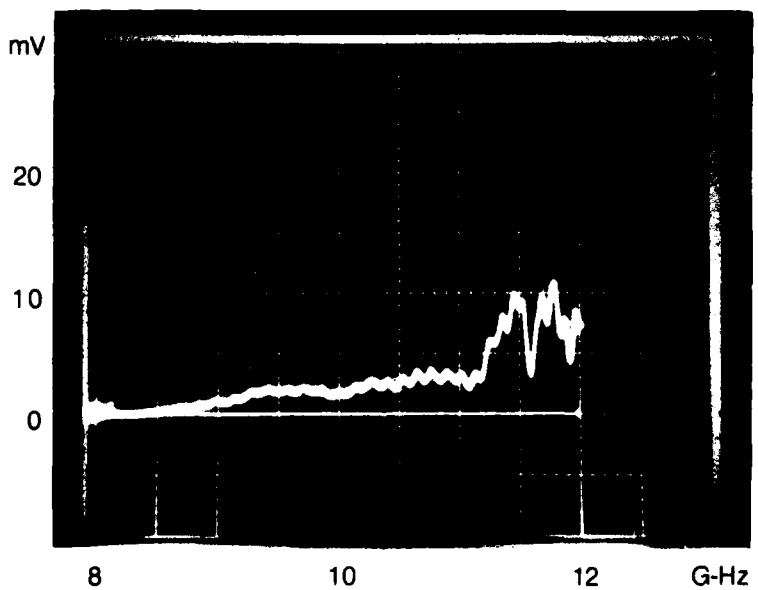

Figure C-4. Frequency response of a polystyrene microwave antenna/ TEA laser cavity.

82-10-18-1